FOR HISTORY-DEPENDENT MATERIALS AND THEIR
NUMERICAL SOLUTION

by L. HAKIM

(*Department of Computing, Imperial College, London,* SW7 2AZ)

and

S. E. MIKHAILOV[†]

(*Department of Mathematical Sciences, Brunel University London, Uxbridge* UB8 3PH)

Summary

A nonlinear history-dependent cohesive zone (CZ) model of quasi-static crack propagation in linear elastic and viscoelastic materials is presented. The viscoelasticity is described by a linear Volterra integral operator in time. The normal stress on the CZ satisfies the history-dependent yield condition, given by a nonlinear Abel-type integral operator. The crack starts propagating, breaking the CZ, when the crack tip opening reaches a prescribed critical value. A numerical algorithm for computing the evolution of the crack and CZ in time is discussed along with some numerical results.

1. Introduction

The cohesive zone (CZ) in a material is the area between two separating but still sufficiently close surfaces ahead of the crack tip, see the shaded regions in Fig. 1. The cohesive forces at the cohesive zones pull the CZ faces together, while the external load applied to the body, on the contrary, causes the crack faces and CZ faces to move further apart and the crack to propagate. When the crack propagates, the cohesive forces vanish at the points where the opening reaches a critical value and these points become the crack surface points, while the new material points, where the history-dependent normalised equivalent stress reaches a critical value, join the CZ. So, the CZ is effectively attached to the crack tip ahead of the crack and moves with the crack, keeping the normalised equivalent stress finite in the body. Note that in what follows, we will refer to the region between $-\hat{a}$ to $\hat{a}$ in Fig. 1 as *crack*, which thus does not include the CZ regions $(-\hat{c}, -\hat{a})$ and $(\hat{a}, \hat{c})$.

One of the most popular CZ models for elasto-perfectly plastic materials is the Leonov–Panasyuk–Dugdale (LPD) model (**1**, **2**). In the LPD model, the maximal normal stress in the CZs is constant and is equal to the material yield stress, $\sigma = \sigma_y$. Some generalisations of this model to viscoelastic materials have been developed. In (**3**, Section 6.2.3), an approximate solution for the LPD model for a linear viscoelastic bulk material with constant $\sigma = \sigma_y$ on the CZ is presented. Wnuk and Knauss (**4**) dealt with a penny-shaped crack in a linear viscoelastic bulk material with the ideally rigid plasticity on the cohesive zone where the yield modulus depends on the CZ tip strain history. In (**5**), an energy approach was implemented to the CZ model with constant stress on the cohesive
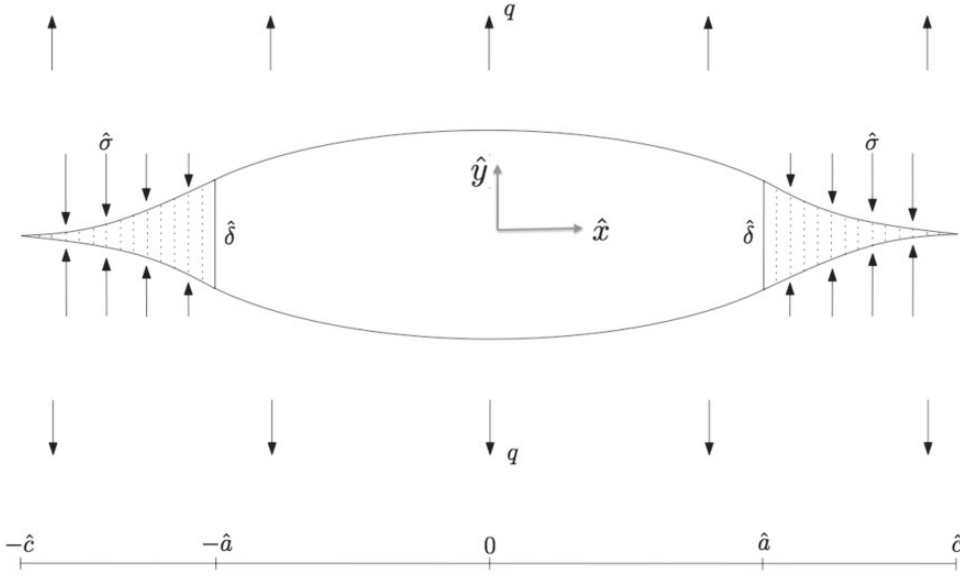

[†]<sergey.mikhailov@brunel.ac.uk>

Fig. 1   Crack with CZs

(failure) zone in a nonlinear viscoelastic bulk material, while in (**9**) with an exponential dependence of the CZ stress on the displacement jump, in a linear viscoelastic bulk material. The CZ models with non-constant CZ stress are sometimes associated with the Barenblatt CZ model (**6**)–(**8**); see also (**3**, section 5.3). Several generalisations to time and history-dependent materials of the CZ models with non-constant stresses and different constitutive relations between the stress and displacement jump were developed (**9**)–(**14**).

The three main components of the LPD-type CZ models are: (i) the constitutive equations in the bulk of the material; (ii) the constitutive equations in the CZ; and (iii) the criterion for the CZ to break, that is, for the crack to propagate.

The model presented in this article is an extension of the LPD model to linear viscoelastic materials with nonlinear history-dependent constitutive equations in the CZ. The history-dependent CZ models can be traced back to (**4**) but, unlike that paper, the history dependence in our article is given by a recently developed normalised equivalent stress (**15**) based on the durability diagram of the bulk material, while the yield condition relates locally with the stress history of considered CZ points instead of being approximated by the history at the CZ tip only. This makes our model more physically consistent and allows to determine its main parameters from the experiments on durability of the bulk of the material, exhibiting history-dependent (creep) behaviour like polymers, concrete or metals under elevated temperature.

The crack starts propagating, when the crack tip opening reaches a critical value (as in the classical LPD model). Our aim is to find the time evolution of the CZ before the crack starts propagating, the delay time (otherwise known as initiation time or crack start time), after which the crack will start to propagate, and to study the further time evolution of the crack and the CZ. In all these stages we assume the quasi-static evolution of crack and CZs, that is, dynamic effects are not considered. Some preliminary results on this model were published in (**16**).

To obtain the solutions, appropriate numerical algorithms were implemented to solve the obtained nonlinear integro-differential problem and the solution convergence is discussed.

2. Problem formulation

Let us consider the two-dimensional problem, with geometry as in Fig. 1. The straight crack occupies the interval $[-\hat{a}(\hat{t}), \hat{a}(\hat{t})]$ and the CZs occupy the intervals $[-\hat{c}(\hat{t}), -\hat{a}(\hat{t})]$ and $[\hat{a}(\hat{t}), \hat{c}(\hat{t})]$ in an infinite linearly elastic or viscoelastic plane loaded at infinity, $\hat{y} = \pm\infty$, in the direction normal to the crack by a traction $\hat{q}$, which is constant in $\hat{x}$, applied at the time $\hat{t} = 0$ and kept constant in time thereafter. The crack is traction-free, $\hat{\sigma}_{\hat{y}\hat{y}}(\hat{x}, 0, \hat{t}) = 0$ for $|\hat{x}| < \hat{a}(\hat{t})$. The initial CZ is absent, that is, the CZ tip coordinates coincide with the crack tip coordinates, which are prescribed, $\hat{c}(0) = \hat{a}(0) = \hat{a}_0$, while the functions $\hat{c}(\hat{t})$ and $\hat{a}(\hat{t})$ for time $\hat{t} > 0$ are to be found. The origin of the Cartesian frame is in the centre of the crack and the $\hat{x}$-axis is directed along the crack.

Thus, (i) the bulk of the material is linearly elastic or viscoelastic, and we now consider item (ii) from our list in the introduction, the constitutive equations on the CZ, while item (iii) regarding the criterion for the CZ to break will be discussed in Section 6.

Following (15), let us introduce at any material point the normalised history-dependent equivalent stress

$$\underline{\Delta}(\hat{\boldsymbol{\sigma}}; \hat{t}) = \left(\frac{\gamma}{\hat{\sigma}_0^\beta} \int_0^{\hat{t}} |\hat{\boldsymbol{\sigma}}(\hat{\tau})|^\beta (\hat{t} - \hat{\tau})^{\gamma-1} d\hat{\tau} \right)^{1/\beta}, \tag{2.1}$$

where $|\hat{\boldsymbol{\sigma}}|$ is the maximum of the principal stresses, and $\hat{t}$ denotes time. Note that stress and time here are physical variables (further on in this section, we will normalise them.) Further, $\gamma = \beta/b$, while the material parameters b, β and $\hat{\sigma}_0$ are introduced as follows.

The parameters $\hat{\sigma}_0 > 0$ and $b > 0$ are material constants in the assumed power-type relation

$$\hat{t}_\infty = \left(\hat{q}/\hat{\sigma}_0 \right)^{-b} \tag{2.2}$$

between the rupture time $\hat{t}_\infty = \hat{t}_\infty(\hat{q})$ and the constant uniaxial tensile stress $\hat{q}$ applied to a sample without cracks. These parameters can be obtained by fitting creep durability experimental data on macro-samples. Here, b is dimensionless, $\hat{t}_\infty$ has units of time (seconds, s) and if the stress $\hat{q}$ is in Pascals (Pa), then $\hat{\sigma}_0$ has units Pa·s$^{1/b}$. For many structural materials the parameter b is in the range between 5 and 20; see (15) and references therein, as well as Appendix A of this article.

The dimensionless parameter $\beta > 0$ is a material constant characterising nonlinearity of the accumulation rule for durability under variable load and can be obtained by fitting experimental data on durability under step-like loading (15). In (15), it is also shown that the accumulation rule (2.1) becomes equivalent to the Robinson rule of linear summation of the partial life times, when $\beta = b$. Thus, for the Robinson rule, evidently, $\gamma = 1$.

We will replace the classical LPD CZ (yield) stress condition, $\hat{\sigma} = \sigma_{\text{yield}}$, with the history-dependent condition

$$\underline{\Delta}(\hat{\boldsymbol{\sigma}}; \hat{t}) = 1, \tag{2.3}$$

while in the rest (the bulk) of the material the strength (non-yield) condition

$$\underline{\Delta}(\hat{\boldsymbol{\sigma}}; \hat{t}) < 1$$

should be satisfied. Relations (2.1) and (2.3), presented in (15), allow us to predict the time- and history-dependent rupture of materials without introduction of a damage measure as an internal

variable and operate only with observable variables and experimentally measurable parameters. Note that the alternative approach, employing internal variables for damage description of CZs, is also possible ([12], [17]).

Relations (2.1) and (2.3) were implemented in ([18]) and ([19]) to solve a similar crack propagation problem without CZ, that is, it was assumed that when condition (2.3) is reached at a material point, this point becomes part of the crack. However, such approach appeared to be applicable only for $b < 2$ (see Appendix 3.2 below), while for many structural materials this parameter is much higher. In this article, a CZ approach is developed instead, to cover the larger range of b values relevant to structural materials. In the CZ approach, when condition (2.3) is reached at a point, this point becomes not yet part of the crack, as in ([18]) and ([19]), but part of the CZ; to become part of the crack, another condition (on the CZ opening) should be satisfied.

As proved further, in Section 3.2, the CZ defined by (2.1), (2.3) can exist only if $0 < \gamma < 1$, that is, $0 < \beta < b$. Note that in all cases considered in ([15]), where these parameters were calculated by fitting the creep durability experimental data, it was found that $0 < \beta < b$, that is, $0 < \gamma < 1$. Thus, we will further consider γ from this interval only.

Assuming that $\hat{\sigma}(\hat{x}, \hat{\tau}) := \hat{\sigma}_{\hat{y}\hat{y}}(\hat{x}, 0, \hat{\tau})$ is non-negative and is the maximal component of the stress tensor ahead of the crack, the CZ condition (2.3)-(2.1) at a point $\hat{x}$ on the CZ at time $\hat{t}$ can be rewritten as

$$\int_{\hat{t}_c(\hat{x})}^{\hat{t}} \hat{\sigma}^\beta(\hat{x}, \hat{\tau})(\hat{t} - \hat{\tau})^{\gamma-1} d\hat{\tau} = \frac{\hat{\sigma}_0^\beta}{\gamma} - \int_0^{\hat{t}_c(\hat{x})} \hat{\sigma}^\beta(\hat{x}, \hat{\tau})(\hat{t} - \hat{\tau})^{\gamma-1} d\hat{\tau}, \tag{2.4}$$

for $\hat{t} \geq \hat{t}_c(\hat{x})$ and $\hat{a}(\hat{t}) \leq |\hat{x}| \leq \hat{c}(\hat{t})$. Here, $\hat{t}_c(\hat{x})$ denotes the time when the point $\hat{x}$ joined the CZ. Equation (2.4) is an inhomogeneous linear Volterra integral equation of the Abel type with unknown function $\hat{\sigma}^\beta(\hat{x}, \hat{t})$ for $\hat{t} \geq \hat{t}_c(\hat{x})$.

Let us first consider the case of linear elastic constitutive equations for the bulk of the material. Applying the results of Muskhelishvili ([20], Section 120), we have for the stresses ahead of the CZ in the elastic material,

$$\hat{\sigma}(\hat{x}, \hat{t}) = \frac{\hat{x}}{\sqrt{\hat{x}^2 - \hat{c}^2(\hat{t})}} \left(\hat{q} - \frac{2}{\pi} \int_{\hat{a}(\hat{t})}^{\hat{c}(\hat{t})} \frac{\sqrt{\hat{c}^2(\hat{t}) - \hat{\xi}^2}}{\hat{x}^2 - \hat{\xi}^2} \hat{\sigma}(\hat{\xi}, \hat{t}) d\hat{\xi} \right), \quad |\hat{x}| > \hat{c}(\hat{t}). \tag{2.5}$$

As one can see from (2.5), $\hat{\sigma}(\hat{x}, \hat{t})$ has generally a square root singularity as $\hat{x}$ tends to the CZ tip $\hat{c}$. The stress intensity factor, $\hat{K}$, at this singularity can be obtained by multiplying (2.5) by $\sqrt{(2\pi[\hat{x} - \hat{c}(\hat{t})])}$ and taking the limit as $\hat{x}$ tends to $\hat{c}(\hat{t})$, which yields

$$\hat{K}(\hat{c}(\hat{t}), \hat{t}) = \sqrt{\pi \hat{c}(\hat{t})} \left(\hat{q} - \frac{2}{\pi} \int_{\hat{a}(\hat{t})}^{\hat{c}(\hat{t})} \frac{\hat{\sigma}(\hat{\xi}, \hat{t})}{\sqrt{\hat{c}^2(\hat{t}) - \hat{\xi}^2}} d\hat{\xi} \right).$$

A sufficient condition for the normalised equivalent stress, Λ, to have no such singularity at the CZ tip is that the stress $\hat{\sigma}$ given by (2.5) does not have it either, while the necessary condition for the latter is that the stress intensity factor, $\hat{K}$, is zero there.

To simplify the equations, we will employ the following normalisations:

$$t = \frac{\hat{t}}{\hat{t}_\infty}, \quad x = \frac{\hat{x}}{\hat{a}_0}, \quad a(t) = \frac{\hat{a}(t\,\hat{t}_\infty)}{\hat{a}_0}, \quad c(t) = \frac{\hat{c}(t\,\hat{t}_\infty)}{\hat{a}_0},$$

$$\sigma(x,t) = \frac{\hat{\sigma}(x\,\hat{a}_0, t\,\hat{t}_\infty)}{\hat{q}}, \quad K(c,t) = \frac{\hat{K}(c\,\hat{a}_0, t\,\hat{t}_\infty)}{\hat{q}\sqrt{\hat{a}_0}}, \tag{2.6}$$

where $\hat{t}_\infty = \hat{t}_\infty(\hat{q}) = (\hat{q}/\hat{\sigma}_0)^{-b}$ denotes the (physical) fracture time for an infinite plane without a crack under the same load, $\hat{q}$. The left-hand sides in (2.6) are the normalised (dimensionless) variables.

Then we obtain the following normalised principle equations for the considered problem:
(a) the CZ condition (2.3) reduced to (2.4), in the form

$$\int_{t_c(x)}^t \sigma^\beta(x,\tau)(t-\tau)^{\gamma-1}d\tau = \frac{1}{\gamma} - \int_0^{t_c(x)} \sigma^\beta(x,\tau)(t-\tau)^{\gamma-1}d\tau \quad \text{for } a(t) \le |x| \le c(t),\ t > t_c(x); \tag{2.7}$$

(b) the expression for the stress ahead of the CZ:

$$\sigma(x,t) = \frac{x}{\sqrt{x^2 - c^2(t)}} \left(1 - \frac{2}{\pi} \int_{a(t)}^{c(t)} \frac{\sqrt{c^2(t) - \xi^2}}{x^2 - \xi^2} \sigma(\xi,t)d\xi \right) \quad \text{for } |x| > c(t); \tag{2.8}$$

(c) the zero stress intensity factor, $K(c,t) = 0$ for $t > 0$, where

$$K(c(t),t) = \sqrt{\pi c(t)} - 2\sqrt{\frac{c(t)}{\pi}} \int_{a(t)}^{c(t)} \frac{\sigma(\xi,t)}{\sqrt{c^2(t) - \xi^2}}d\xi. \tag{2.9}$$

3. Some analytical results

3.1 *Analytical solution of the Abel-type equation in the cohesive zone*

To obtain the stresses in the CZ, we have to solve the Abel-type linear integral equation (2.7) for $\sigma^\beta(x,t)$ at $t \ge t_c$, when $\sigma^\beta(x,\tau)$ is known at $\tau \in [0, t_c(x)]$ at its right-hand side. To this end, we have the following important assertion, see for example (**21**, Theorem 1.2.1).

THEOREM 1. *If $f(t)$ is absolutely continuous on $[t_c, T_1]$, then the Abel type integral equation*

$$\int_{t_c}^t g(\tau)(t-\tau)^{\gamma-1}d\tau = f(t), \quad t \in [t_c, T_1], \quad \gamma \in (0,1)$$

has a unique solution g in $L_1(t_c, T_1)$, which is given by formula

$$g(\tau) = \frac{\sin(\pi\gamma)}{\pi} \frac{d}{d\tau} \int_{t_c}^\tau f(t)(\tau - t)^{-\gamma}dt. \tag{3.1}$$

Integrating by parts, expression (3.1) can be written as

$$g(\tau) = \frac{\sin(\pi\gamma)}{\pi}\left(f(t_c)(\tau - t_c)^{-\gamma} + \int_{t_c}^{\tau} f'(t)(\tau - t)^{-\gamma}dt\right). \tag{3.2}$$

For equation (2.7),

$$f(t) = \frac{1}{\gamma} - \int_0^{t_c} \sigma^\beta(x, \tau)(t - \tau)^{\gamma-1}d\tau.$$

Moreover, we know that $f(t_c) = 0$ when $t_c > 0$, since the condition $\Lambda = 1$ (see (2.7)) is satisfied at $t = t_c > 0$. Finally, $\sigma^\beta(x, \tau) = g(\tau)$ at $\tau \geq t_c$.

3.2   *Material parameter range of CZ model applicability*

To analyse the range of $\gamma = \beta/b$, for which the CZ model based on conditions (2.1), (2.3) can exist, let us first remark that if $\gamma = 1$, then

$$\frac{d}{d\hat{t}}\underline{\Lambda}(\hat{\boldsymbol{\sigma}}; \hat{t}) = \frac{1}{b\hat{\sigma}_0^\beta}\underline{\Lambda}^{1-\beta}(\hat{\boldsymbol{\sigma}}; \hat{t})|\hat{\boldsymbol{\sigma}}(\hat{t})|^\beta,$$

which means that $\underline{\Lambda}(\hat{\boldsymbol{\sigma}}; \hat{t})$ is a strictly growing function for any $\hat{t}$, when $|\hat{\boldsymbol{\sigma}}(\hat{t})| \neq 0$. Particularly, if the cohesive condition (2.3) is reached at some point $\hat{x}$ in time $\hat{t}_c(\hat{x})$, it can not stay at larger times, $\hat{t} > \hat{t}_c(\hat{x})$ unless $\hat{\boldsymbol{\sigma}}(\hat{x}, \hat{t}) = 0$; but if $|\hat{\boldsymbol{\sigma}}(\hat{x}, \hat{t})| = 0$ for $t > t_c(\hat{x})$ this means that the point $\hat{x}$ belongs to the crack rather than to the CZ. That is, the CZ can not exist at $\gamma = 1$, corresponding to the Robinson damage linear accumulation rule. Instead, the Robinson rule implies the crack propagation without the CZ, which, as follows from (22, 18, 19), is possible only if $0 < b < 2$ since for $b \geq 2$ the Volterra integral in the model becomes strongly singular and thus divergent. Note however, the Neuber–Novozhilov-type non-local approach extends the applicability range of the Robinson rule for cracks to arbitrary $b > 0$, see (22, 18).

Similarly, if $\gamma > 1$, then

$$\frac{d}{d\hat{t}}\underline{\Lambda}(\hat{\boldsymbol{\sigma}}; \hat{t}) = \frac{\gamma}{\beta\hat{\sigma}_0^\beta}\underline{\Lambda}^{1-\beta}(\hat{\sigma}; \hat{t})\int_0^{\hat{t}}|\hat{\boldsymbol{\sigma}}(\hat{\tau})|^\beta(\hat{t} - \hat{\tau})^{\gamma-2}d\hat{\tau} > 0,$$

which also prevents for the CZ condition (2.3) to hold at any time $\hat{t} > \hat{t}_c(\hat{x})$, after the condition had been reached at a time $\hat{t}_c(\hat{x})$, even if $\sigma(\hat{x}, \hat{t}) = 0$ for $\hat{t} > \hat{t}_c(\hat{x})$.

Thus, the CZ model defined by (2.1), (2.3) is applicable only if $0 < \gamma < 1$, that is, $0 < \beta < b$. Note that the material parameters obtained in (15) by fitting experimental data for several structural materials satisfy these conditions.

4. CZ growth for the stationary crack

In this section, we will consider the stationary stage, when the crack length is constant, $a(t) = a(0) = 1$, and only the CZ grows with time. Our aim here is to find the CZ tip position

evolution in time, $c(t)$. In Section 6, we implement the crack propagation criterion, and the stationary stage will hold during the so-called delay time, being followed by the crack propagation stage.

4.1 *Numerical method for $c(t)$*

Let us introduce a time mesh with nodes $t_i = ih$, for $i = 0, 1, 2, 3, \ldots, n$, where $h = 1/n$ is a time increment and $t_n = 1$. At each time step $t_i, i > 0$, we use the secant method to find the roots, $c(t_i) = c_i$, of the equation $K(c_i, t_i) = 0$, as follows:

1. Take two initial approximations, c_{i1} and c_{i2}, for $c(t_i)$.
2. Obtain $K_1 = K(c_{i1}, t_i)$ and $K_2 = K(c_{i2}, t_i)$ using (2.9). To evaluate the integral in (2.9),

$$\int_{a(0)}^{c(t_i)} \frac{1}{\sqrt{c^2(t_i) - \xi^2}} \sigma(\xi, t_i) d\xi, \qquad (4.1)$$

we piecewise linearly interpolate $\sigma(\xi, t_i)$ in ξ on the CZ, over the points $c(t_k), k = 0, 1, 2, \ldots, i$. To obtain $\sigma(c(t_i), t_i)$, we use the Abel integral equation (2.7) with zero left-hand side, which reduces the equation to the following one,

$$\int_0^{t_i} \sigma^\beta(c(t_i), \tau)(t_i - \tau)^{\gamma-1} d\tau = \frac{1}{\gamma}.$$

By explicit integration of the piecewise linear interpolant of the function $\sigma^\beta(c(t_i), \tau)$ in τ over the time instants $t_j, j = 0, 1, 2, \ldots, i$, including the unknown value $\sigma^\beta(c(t_i), t_i)$, we obtain the linear algebraic equation for the latter, which has the solution

$$\sigma^\beta(c(t_i), t_i) = (t_i - t_{i-1})^{-\gamma} \left\{ (\gamma + 1)[1 - \sigma^\beta(c(t_i), 0)t_i^\gamma] \right.$$

$$+ \sum_{j=0}^{i-1} \sigma^\beta(c(t_i), t_j) \frac{(t_i - t_j)^{\gamma+1} - (t_i - t_{j+1})^{\gamma+1}}{t_{j+1} - t_j}$$

$$\left. + \sum_{j=1}^{i-1} \sigma^\beta(c(t_i), t_j) \frac{(t_i - t_j)^{\gamma+1} - (t_i - t_{j-1})^{\gamma+1}}{t_j - t_{j-1}} \right\}, \quad i > 0. \quad (4.2)$$

To obtain $\sigma(c(t_k), t_i)$, at each $k < i$, we use (2.7) with $x = c(t_k), t_c(x) = t_k$ and $t = t_i > t_k$. First, we again evaluate the right-hand side integral $\int_0^{t_k} \sigma^\beta(x, \tau)(t - \tau)^{\gamma-1} d\tau$ by analytic integration of the piecewise linear interpolant of the function $\sigma^\beta(x, \tau)$ in τ over the time instants $t_j, j = 0, 1, 2, ..., k$, where $t_0 = 0$. Then we use the analytical solution (3.2) of the integral equation (2.7) and arrive at

the following solution at $t > t_k$ for $x = c(t_k)$,

$$
\sigma^\beta(x, t) = -\frac{1}{\pi} \sin(\pi\gamma) \sum_{j=1}^{k} \left\{ \sigma^\beta(x, t_{j-1}) \left[V(t_{j-1}, t, t_k) - V(t_j, t, t_k) \right] \right.
$$

$$
+ \frac{\sigma^\beta(x, t_j) - \sigma^\beta(x, t_{j-1})}{\gamma(t_j - t_{j-1})} \left[W(t_{j-1}, t, t_k) - W(t_j, t, t_k) - \gamma(t_j - t_{j-1}) V(t_j, t, t_k) \right] \right\}
$$

$$
= -\frac{1}{\pi} \sin(\pi\gamma) \sum_{j=1}^{k} \left\{ \sigma^\beta(x, t_{j-1}) \left[\widetilde{V}(t_{j-1}, t, t_k) - \widetilde{V}(t_j, t, t_k) \right] \right.
$$

$$
+ \frac{\sigma^\beta(x, t_j) - \sigma^\beta(x, t_{j-1})}{\gamma(t_j - t_{j-1})} \left[\widetilde{W}(t_{j-1}, t, t_k) - \widetilde{W}(t_j, t, t_k) - \gamma(t_j - t_{j-1}) \widetilde{V}(t_j, t, t_k) \right] \right\}
$$

$$
= -\operatorname{sinc}(\pi\gamma) \left\{ \sigma^\beta(x, 0) \left[\widetilde{\widetilde{V}}_0(t, t_k) + \frac{\widetilde{W}(t_1, t, t_k) - \widetilde{W}(0, t, t_k)}{t_1} \right] + \sigma^\beta(x, t_k) \frac{\widetilde{W}(t_{k-1}, t, t_k)}{t_k - t_{k-1}} \right.
$$

$$
+ \sum_{j=1}^{k-1} \sigma^\beta(x, t_j) \left[\frac{\widetilde{W}(t_{j+1}, t, t_k) - \widetilde{W}(t_j, t, t_k)}{t_{j+1} - t_j} - \frac{\widetilde{W}(t_j, t, t_k) - \widetilde{W}(t_{j-1}, t, t_k)}{t_j - t_{j-1}} \right] \right\}
$$

$$
= -\operatorname{sinc}(\pi\gamma) \left\{ \sigma^\beta(x, 0) \widetilde{\widetilde{V}}_0(t, t_k) + \frac{\sigma^\beta(x, t_1) - \sigma^\beta(x, 0)}{t_1} \widetilde{W}(0, t, t_k) \right.
$$

$$
+ \sum_{j=1}^{k-1} \left[\frac{\sigma^\beta(x, t_{j+1}) - \sigma^\beta(x, t_j)}{t_{j+1} - t_j} - \frac{\sigma^\beta(x, t_j) - \sigma^\beta(x, t_{j-1})}{t_j - t_{j-1}} \right] \widetilde{W}(t_j, t, t_k) \right\}, \quad (4.3)
$$

where

$$
V(y, t, t_c) = \int_{t_c}^{t} \frac{(\tau - y)^{\gamma-1}}{(t - \tau)^\gamma} d\tau = \pi \csc(\pi\gamma) + \widetilde{V}(y, t, t_c), \tag{4.4}
$$

$$
\widetilde{V}(y, t, t_c) = -\frac{1}{\gamma} \left(\frac{t_c - y}{t - y} \right)^\gamma {}_2F_1 \left[\gamma, \gamma; 1 + \gamma; \frac{t_c - y}{t - y} \right], \tag{4.5}
$$

$$
\widetilde{\widetilde{V}}_0(t, t_k) = \gamma \widetilde{V}(0, t, t_c) = -\left(\frac{t_c}{t} \right)^\gamma {}_2F_1 \left[\gamma, \gamma; 1 + \gamma; \frac{t_c}{t} \right], \tag{4.6}
$$

$$
W(y, t, t_c) = \int_{t_c}^{t} \frac{(\tau - y)^\gamma}{(t - \tau)^\gamma} d\tau = \gamma\pi \csc(\pi\gamma)(t - y) + \widetilde{W}(y, t, t_c), \tag{4.7}
$$

$$
\widetilde{W}(y, t, t_c) = -\frac{1}{1 + \gamma}(t_c - y)^{1+\gamma}(t - y)^{-\gamma} {}_2F_1 \left[1 + \gamma, \gamma; 2 + \gamma; \frac{t_c - y}{t - y} \right], \tag{4.8}
$$

$_2F_1$ is the Gauss hypergeometric function and $\operatorname{sinc}(x) = (\sin x)/x$.

To implement (4.2) and (4.3), we need, in turn, to find $\sigma(c(t_k), t_j)$ for $0 \le t_j < t_k \le t_i$ from (2.8) (since $c(t_j) < c(t_k)$), $j = 0, 1, \ldots, k - 1$. For $j = 0$, we have $t_0 = 0$ and the integral in (2.8)

vanishes giving

$$\sigma(x, 0) = \frac{x}{\sqrt{x^2 - 1}} \quad \text{for } |x| > 1, \ j = 0. \tag{4.9}$$

For $j > 0$, taking into account that $K(c(t_j), t_j) = 0$, (2.8) reduces to

$$\sigma(x, t) = \frac{2x}{\pi} \sqrt{x^2 - c^2(t_j)} \int_{a(t)}^{c(t_j)} \frac{\sigma(\xi, t_j)}{(x^2 - \xi^2)\sqrt{c^2(t_j) - \xi^2}} \, d\xi \quad \text{for } |x| > c(t_j), \ j > 0, \tag{4.10}$$

where the integral is calculated, similarly to integral (4.1), linearly interpolating $\sigma(\xi, t_j)$ between $\xi = c(t_m)$ and $\xi = c(t_{m+1})$ for $m = 0, 1, \ldots, j - 1$.

3. Find the next approximation for c_i using

$$(c_i)_3 = \frac{K_2 \cdot c_{i1} - K_1 \cdot c_{i2}}{K_2 - K_1}$$

4. If $|(c_i)_3 - c_{i1}| < \varepsilon$ or $|(c_i)_3 - c_{i2}| < \varepsilon$ then convergence is reached and we allocate $c(t_i) = c_3$ and go to the step $t = t_{i+1}$; otherwise, take the new c_{i1} or c_{i2} as $(c_i)_3$ and return to step 2 above. Here ε is some tolerance.

4.2 Numerical results for the stationary crack

The described algorithm was implemented in MATLAB with $\varepsilon = 10^{-8}$ as the tolerance value. The graphs on Figs 2–6 show the obtained numerical results on the evolution of the CZ tip position as well as the stress distribution on the CZ for various mesh sizes.

The graphs in Fig. 2 (left) show that the CZ length ahead of the stationary crack is monotonically and continuously increasing with time. From Fig. 3 we can see that the stress at a material point ahead of the CZ is growing monotonically in time t, peaking at the time t^* when the point becomes
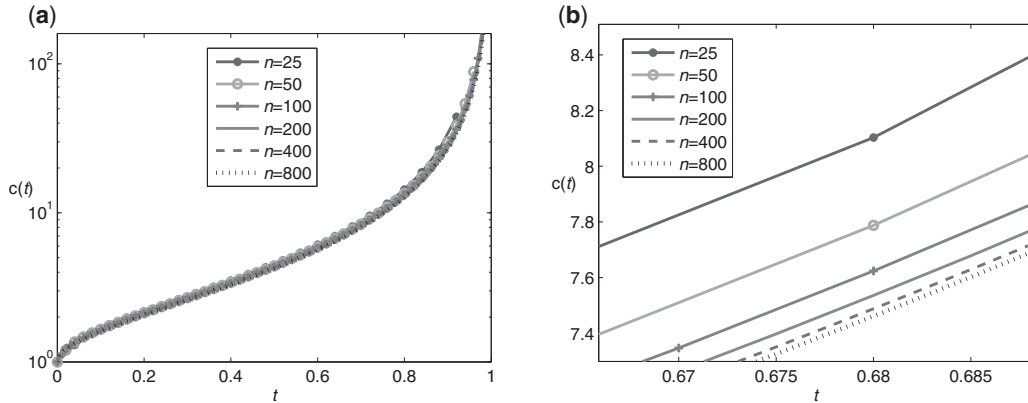

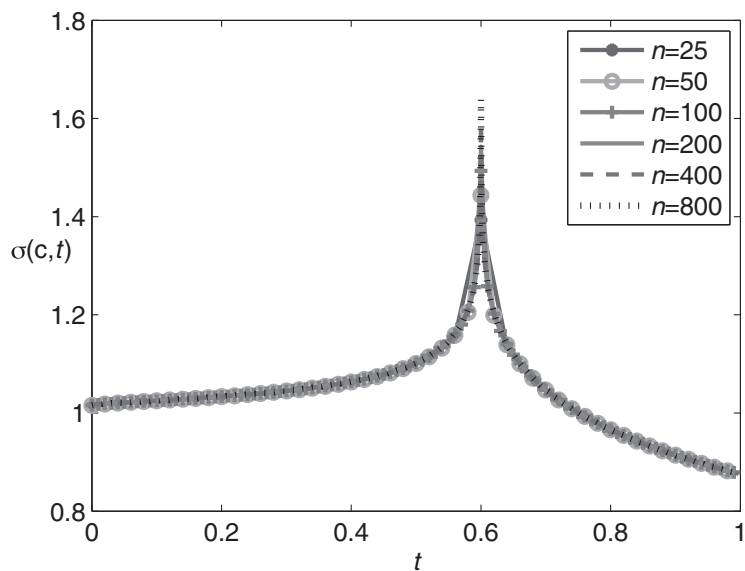Fig. 2   CZ tip position versus time for $b = 4$, $\beta = 2$ and different meshes

Fig. 3 $\sigma(c(t^*), t)$ versus time for $b = 4$, $\beta = 2$, $t^* = 0.6$: global picture for different meshes
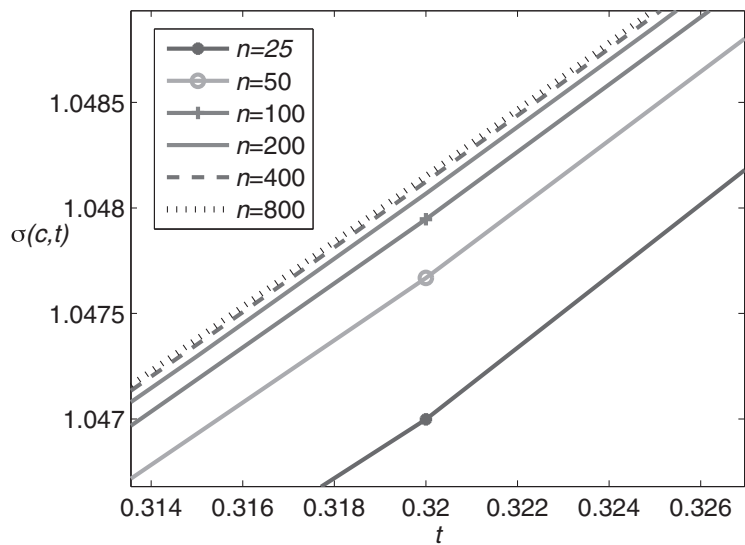

Fig. 4 $\sigma(c(t^*), t)$ for $b = 4$, $\beta = 2$, $t^* = 0.6$: zoomed ahead of the CZ ($t < t^*$) for different meshes
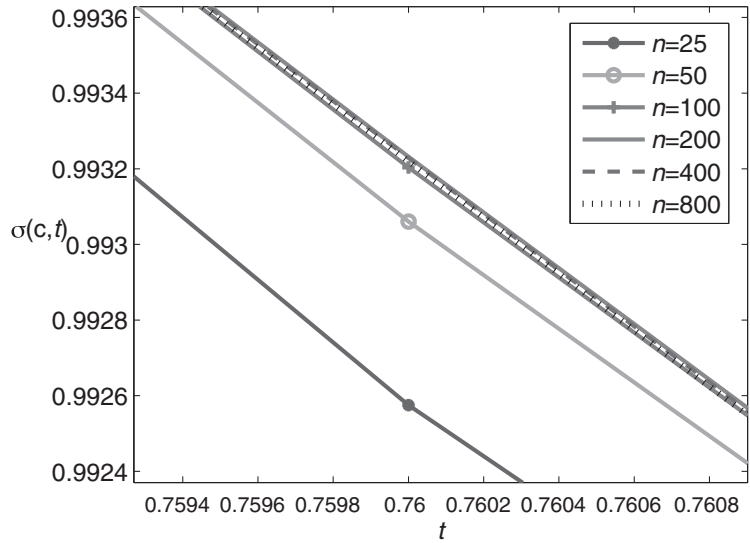
Fig. 5 $\sigma(c(t^*), t)$ for $b = 4$, $\beta = 2$, $t^* = 0.6$: zoomed in the CZ ($t > t^*$) for different meshes
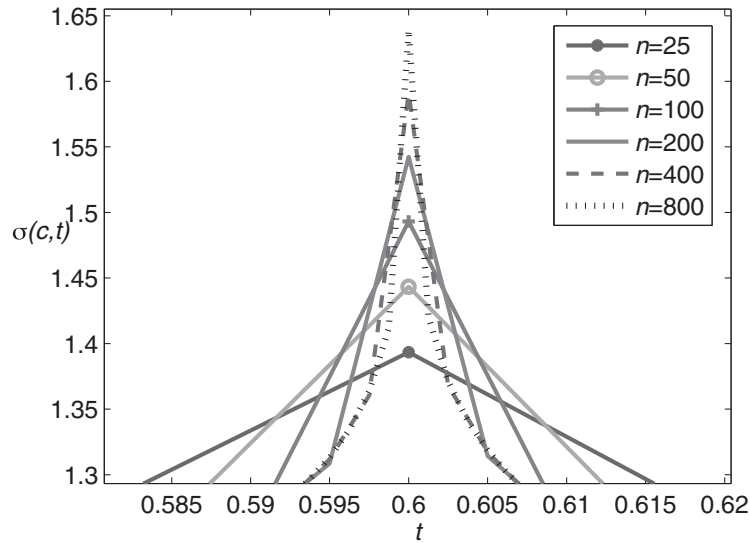

Fig. 6 $\sigma(c(t^*), t)$ for $b = 4$, $\beta = 2$, $t^* = 0.6$: zoomed at the CZ tip (near t^*) for different meshes

the CZ tip, and then monotonically decreasing inside the CZ. The graphs in Fig. 2 (right) and in Figs 4–6 illustrate fast numerical convergence of the obtained results as the mesh is refined (the time step $h = 1/n$ is decreased), except maybe the graphs in Fig. 6 for the stress σ at the CZ tip. The convergence is analysed quantitatively in Section 7 and in more detail in (23).

5. Crack tip opening

5.1 *General equations for the crack tip opening*

We will first consider the case when the bulk of the material is linearly elastic and then convert the obtained solution to the case of linear viscoelastic materials using the so-called Volterra principle. Using the representations by Muskhelishvili (20, section 120), it can be deduced that in the linearly elastic isotropic homogeneous plane with a crack, the normal displacement jump at a point $\hat{x}$ on the crack or CZ is

$$[\hat{u}_e](\hat{x}, \hat{t}) = [\hat{u}_e^{(q)}](\hat{x}, \hat{t}) + [\hat{u}_e^{(\sigma)}](\hat{x}, \hat{t}), \quad |\hat{x}| < \hat{c}(t),$$

where

$$[\hat{u}_e^{(q)}](\hat{x}, \hat{t}) = \frac{\hat{q}}{2M_0}\sqrt{\hat{c}(\hat{t})^2 - \hat{x}^2}, \quad [\hat{u}_e^{(\sigma)}](\hat{x}, \hat{t}) = \frac{1}{2\pi M_0}\int_{\hat{a}(\hat{t})}^{\hat{c}(\hat{t})} \hat{\sigma}(\hat{\xi}, \hat{t})\Gamma(\hat{x}, \hat{\xi}; \hat{c}(\hat{t}))d\hat{\xi},$$

and

$$\Gamma(\hat{x}, \hat{\xi}; \hat{c}) = \ln\left[\frac{2\hat{c}^2 - \hat{\xi}^2 - \hat{x}^2 - 2\sqrt{(\hat{c}^2 - \hat{x}^2)(\hat{c}^2 - \hat{\xi}^2)}}{2\hat{c}^2 - \hat{\xi}^2 - \hat{x}^2 + 2\sqrt{(\hat{c}^2 - \hat{x}^2)(\hat{c}^2 - \hat{\xi}^2)}}\right].$$

In the above expressions, $M_0 = \mu_0/(1 + \varkappa)$, $\varkappa = 3 - 4\nu$ under the plane strain condition, while $\varkappa = (3 - \nu)/(1 + \nu)$ under the plane stress condition, $\mu_0 = E/[2(1 + \nu)]$ is the shear modulus, where E and ν denote Young's modulus of elasticity and Poisson's ratio, respectively.

Then the displacement jump at the crack tip, that we call the crack tip opening, for elastic material is given by the formula

$$\hat{\delta}_e(\hat{t}) := [\hat{u}_e](\hat{a}(\hat{t}), \hat{t}) = \frac{1}{2M_0}\left(\hat{q}\sqrt{\hat{c}^2(\hat{t}) - \hat{a}^2(\hat{t})} + \frac{1}{\pi}\int_{\hat{a}(\hat{t})}^{\hat{c}(\hat{t})} \hat{\sigma}(\hat{\xi}, \hat{t})\Gamma(\hat{a}(\hat{t}), \hat{\xi}, \hat{c}(\hat{t}))d\hat{\xi}\right). \tag{5.1}$$

Using the space and time normalisations given in (2.6) as well as the following normalisation for the displacement jumps,

$$[u_e(x, t)] = \frac{2M_0}{\hat{q}}\frac{[\hat{u}_e]\left(\hat{x}\,\hat{a}_0, t\hat{t}_\infty\right)}{\hat{a}_0}, \quad \delta_e(t) = \frac{2M_0}{\hat{q}}\frac{\hat{\delta}_e(t\,\hat{t}_\infty)}{\hat{a}_0}, \tag{5.2}$$

we obtain

$$[u_e](x, t) = \sqrt{c^2(t) - x^2} + \frac{1}{\pi}\int_{a(t)}^{c(t)} \sigma(\xi, t)\Gamma(x, \xi; c(t))d\xi,$$

$$\delta_e(t) = [u_e](a(t), t) = \sqrt{c^2(t) - a^2(t)} + \frac{1}{\pi}\int_{a(t)}^{c(t)} \sigma(\xi, t)\Gamma(a(t), \xi; c(t))d\xi. \tag{5.3}$$

To obtain the crack tip opening in the viscoelastic case, we will implement the so-called Volterra principle, according to which we have to replace the elastic constants μ_0 and ν in the elastic solution by the corresponding viscoelastic operators, to arrive at the viscoelastic solution. Although this approach does not always bring a viscoelastic solution for the problems with moving boundaries, it is possible to show (24) that this approach leads to a viscoelastic solution for the plane symmetric problem with a straight propagating crack. This means that for the viscoelastic problem we can directly use the results by Muskhelishvili for the stress representation given in (2.5) since they do not include the elastic constants at all.

Then, to obtain the crack opening in the viscoelastic case, we have to replace $1/M_0$ in (5.1) by the second kind Volterra integral operator $\boldsymbol{M}^{-1}$ defined as

$$\left(\boldsymbol{M}^{-1}\hat{\sigma}\right)(\hat{t}) = (1+\boldsymbol{\varkappa})\boldsymbol{\mu}^{-1} = \frac{1}{M_0}\left\{\hat{\sigma}\left(\hat{t}\right) + \int_0^{\hat{t}} \mathcal{K}\left(\hat{t} - \hat{\tau}\right)\sigma\left(\hat{\tau}\right)d\hat{\tau}\right\}, \tag{5.4}$$

where the kernel $\mathcal{K}$ and the instant parameter M_0 are known. Particularly, if the viscoelastic material has constant (purely elastic) Poisson's ratio ν (and thus the parameter $\varkappa$), then $M_0 = \mu_0/(1+\varkappa)$ as before, μ_0 is the instant shear modulus, while $\mathcal{K}$ is the derivative, $\dot{\mathcal{J}}$, of the known creep function $\mathcal{J}$. If Poisson's ratio $\boldsymbol{\nu}$ (and thus the parameter $\boldsymbol{\varkappa}$) are not constants but known second-kind Volterra operators, then the kernel $\mathcal{K}$ is determined by the middle part of equation (5.4). Hence, the viscoelastic crack tip opening becomes

$$\hat{\delta}_v\left(\hat{t}\right) = [\hat{u}_v](\hat{a}(\hat{t}), \hat{t}) = \hat{\delta}_e\left(\hat{t}\right) + \int_0^{\hat{t}} \mathcal{K}\left(\hat{t} - \hat{\tau}\right)[\hat{u}_e](\hat{a}(\hat{t}), \hat{\tau})d\hat{\tau}. \tag{5.5}$$

In our numerical examples, we assume

$$\mathcal{K}\left(\hat{t} - \hat{\tau}\right) = (\mu_0/\eta)e^{-(\hat{t}-\hat{\tau})/\hat{\theta}}. \tag{5.6}$$

This can be associated with the case, when Poisson's ratio is constant and $\mathcal{K} = \dot{\mathcal{J}}$, where $\mathcal{J}$ is the creep function of a standard linear solid, while, the material parameters $\hat{\theta}$ and η are, respectively, the relaxation time and the viscosity of the viscoelastic material. Such viscoelastic models satisfactorily describe some polymers, for example, PMMA (Polymethyl methacrylate, also known as plexiglas). After employing the normalised parameters

$$\delta_v(t) = \frac{2M_0\hat{\delta}_v(t\,\hat{t}_\infty)}{\hat{a}_0\hat{q}}, \quad \theta = \frac{\hat{\theta}}{\hat{t}_\infty}, \quad m = \frac{\mu_0\hat{t}_\infty}{\eta}, \tag{5.7}$$

equation (5.5) reduces to the following expression for the normalised crack tip opening in the viscoelastic case,

$$\delta_v(t) = [u_v(a(t), t)] = \delta_e(t) + m\int_{t_c(a(t))}^t e^{-(t-\tau)/\theta}[u_e](a(t), \tau)d\tau, \tag{5.8}$$

where the lower limit of the integral is replaced with $t_c(a(t))$ since $[u_e](x, \tau) = 0$ when $\tau \leq t_c(x)$. In the numerical examples, for the viscoelastic case, we used values $m = 5$ and $\theta = 1$, which are of the order of the ones for PMMA, see Appendix A.

5.2 *Crack tip opening for the stationary crack*

The graphs in Figs 7–8 show the stationary crack tip opening evolution for $b = 4$ and $\beta = 2$, in the elastic and viscoelastic cases for different time meshes, where the right, zoomed graphs indicate a good convergence of the results as the time mesh size, $h = 1/n$ decreases. Figure 9 gives comparison of the crack opening for the cases of elastic and viscoelastic response of the bulk of the material (for the finest mesh, $n = 800$). As expected, since the instant Young modulus of the viscoelastic material is chosen equal to the one in the purely elastic case, the creep in the viscoelastic material, described by the Volterra integral term, makes the crack opening in it higher than in the purely elastic case, at the same time instances.
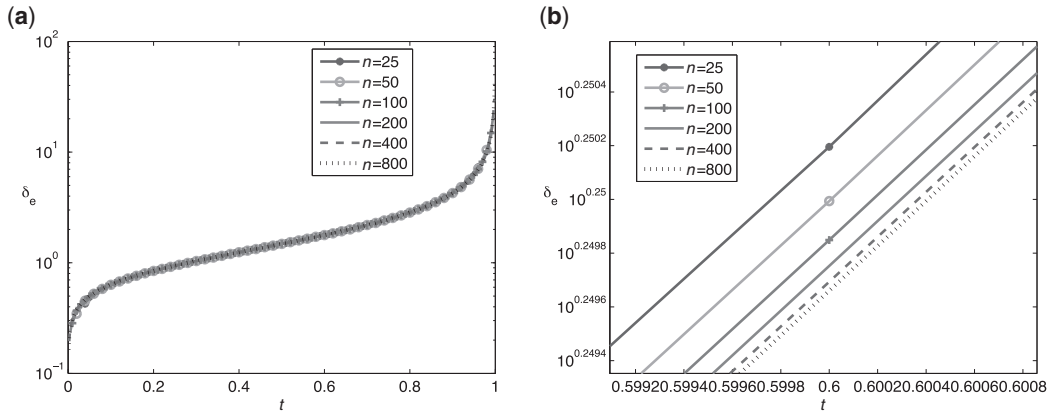
Fig. 7 Crack tip opening δ_e versus time t in the elastic case for different time meshes, $b = 4$ and $\beta = 2$
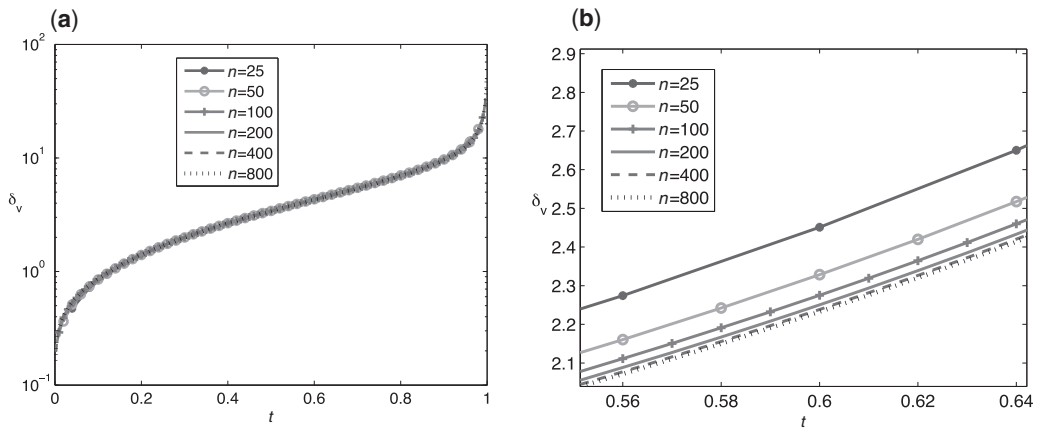
Fig. 8 Crack tip opening δ_v versus time t in the viscoelastic case for different time meshes, for $b = 4$ and $\beta = 2$
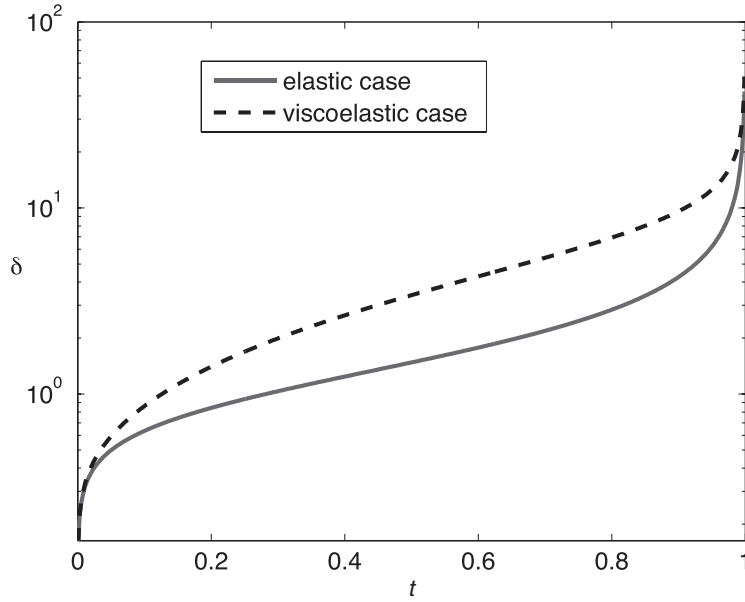
Fig. 9 Comparison of the crack tip opening δ versus time t for elastic and viscoelastic cases, $b = 4$ and $\beta = 2$

6. Crack propagation stage

Let us now consider the crack propagation stage, where the crack tip and the CZ tip will propagate but not necessary at the same rate, that is, the crack length can vary.

6.1 *Delay time*

Further on, we assume the crack will start to propagate when the crack tip opening $\hat{\delta}$ reaches a critical value $\hat{\delta}_c$, considered as a material constant, which is main component (iii) of the LPD-type CZ model given in the introduction. Assuming that the external load $\hat{q}$ is applied at time $\hat{t} = 0$, the time instant, when the crack tip opening reaches a critical value and the crack starts propagating, will be referred to as the fracture delay time (sometimes also named as the fracture initiation time), $\hat{t}_d$.

Similar to (2.6), (5.2) and (5.7), we employ the following normalised parameters,

$$t_d = \frac{\hat{t}_d}{\hat{t}_\infty}, \quad \delta_c = \frac{2\mu_0}{(1 + \varkappa)\hat{q}} \frac{\hat{\delta}_c}{\hat{a}_0}. \tag{6.1}$$

The crack tip opening, $\delta(t)$, satisfies equation

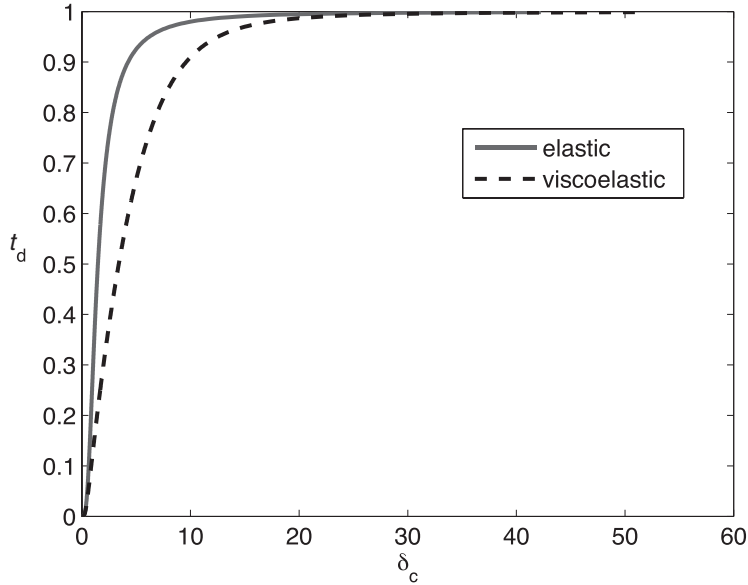$$\delta_e(t) = \delta_c, \quad t \geq t_d. \tag{6.2}$$

Fig. 10   Delay time, t_d, versus critical crack opening, δ_c, for elastic and viscoelastic cases, for $b = 4$ and $\beta = 2$

for the purely elastic case or equation

$$\delta_v(t) = \delta_c, \quad t \geq t_d. \tag{6.3}$$

for the viscoelastic case, where $\delta_e(t_i)$ and $\delta_v(t_i)$ are given by (5.3) and (5.8), respectively.

Equating δ to δ_c on Fig. 9, one can obtain the dependence of t_d on δ_c shown in Fig. 10. One can see from it that, as expected, for sufficiently big critical crack tip opening, δ_c, the delay time approaches the rupture time of the body without crack.

Normalisation formula (6.1) can be rewritten in terms of the initial crack length $\hat{a}_0$ normalised in a special way as

$$\tilde{a}_0 = \frac{(1 + \varkappa)\hat{q}}{2\mu_0} \frac{\hat{a}_0}{\hat{\delta}_c} = \frac{1}{\delta_c}.$$

Then, rearranging Fig. 10 we obtain rather informative graphs in of the dependence of the delay time on the initial crack length, presented in Fig. 11. These graphs clearly show that when the initial crack length tends to zero, the crack delay time tends to a final value, which is the rupture time of the body without crack. This illustrates the applicability of the CZ model to description of the small cracks.

6.2   *Numerical algorithm on the propagating crack stage*

To calculate the crack length and the CZ length at $t > t_d$, we use the uniform time mesh with time steps $t_i = t_d + ih$, where h is the step size, and implement the secant method to solve (6.2) (in the elastic case) or (6.3) (in the viscoelastic case) for $a(t_i)$. To do this, we need $c(t_i)$ at each iteration, which is obtained as in Section 4.1. Further details on the algorithm are given below.
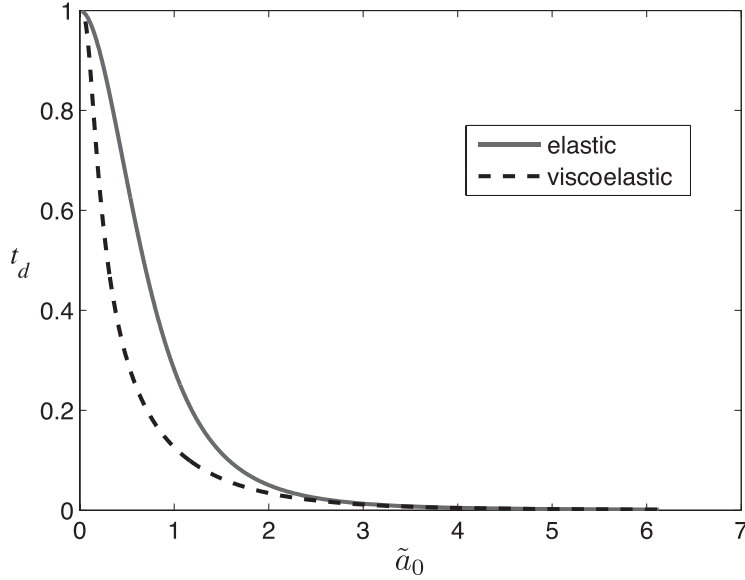
Fig. 11 Delay time, t_d, versus normalised initial crack length, $\tilde{a}_0$, for elastic and viscoelastic cases, for $b = 4$ and $\beta = 2$

6.2.1 *Initial approximations.*   Note that we take the following two initial approximations for $a_i := a(t_i)$: $(a_i)_1 = c_m := c(t_m)$ and $(a_i)_2 = c_{m+1} := c(t_{m+1})$. The index $m < i - 1$ is chosen so that the signs of $\delta_e(t_i) - \delta_c$ (for the elastic case) or $\delta_v(t_i) - \delta_c$ (for the viscoelastic case) are different for $a_i = (a_i)_1$ and $a_i = (a_i)_2$. At the start of crack growth, we begin with $(a_i)_1 = a_0 = c_0$ and $(a_i)_2 = c_1$. The advantage of choosing previous CZ tip positions, c_m, as initial approximations for a_i is that we already know the stress history at these points since they were computed in the previous time steps.

6.2.2 *Computing the stress at a crack tip position.*   Further, during the secant iterations to obtain a_i, we will need to compute the stress $\sigma(a_i, t_i)$ for cases when a_i does not equal to the (previous) c_m values. This stress value will be used for the integration while calculating $K(c_i, t_i)$ and $\delta_e(t_i)$ by (2.9) and (5.3), respectively. Note that we cannot directly use the solution given by (4.3) to solve (2.7) with $x = a_i$, $c_m < a_i < c_{m+1}$, since it needs $t_c(a_i)$, which approximate calculation can be time consuming. Instead, we first find $\sigma^\beta(c_m, t_i)$ and $\sigma^\beta(c_{m+1}, t_i)$ by (4.3) and then employ the following linear interpolation,

$$\sigma^\beta(a_i, t_i) \approx \sigma^\beta(c_m, t_i) + \frac{\sigma^\beta(c_{m+1}, t_i) - \sigma^\beta(c_m, t_i)}{c_{m+1} - c_m}\,(a_i - c_m)\,, \quad c_m < a_i < c_{m+1}.$$

6.2.3 *Calculating the viscoelastic crack tip opening.*   The crack tip opening in the viscoelastic case is given by (5.8). When an approximation for a_i is a previous value of c, $a_i = c_m$, then the integration over τ in (5.8) is from t_m to $t = t_i$. However, when $a_i \neq c(t_m)$, the time instant when a_i became part of the CZ, $t_c(a_i)$, is unknown, and to avoid a time consuming calculation of $t_c(a_i)$, we implement the following approach. We replace $t_c(a_i)$ with t_m, where $c_m < a_i < c_{m+1}$, but take into

account that $[u_e](a_i, t_m) = 0$. The integral over τ will be evaluated by piecewise linearly interpolating $[u_e](a_i, \tau)$ between t_k and t_{k+1} for $k = m, m+1, \ldots, i-1$. Thus, the integral would be written as

$$\sum_{k=m}^{i-1} \int_{t_k}^{t_{k+1}} e^{-(t_i-\tau)/\theta} [u_e](a_i, \tau) d\tau$$

where

$$[u_e](a_i, \tau) \approx [u_e](a_i, t_k) - \frac{[u_e](a_i, t_{k+1}) - [u_e](a_i, t_k)}{t_{k+1} - t_k}(\tau - t_k), \quad t_k < \tau < t_{k+1},$$

and the first non-zero $[u_e](a_i, t_k)$ is for $k = m+1$, when $c_m < a_i < c_{m+1}$.

During implementation of the algorithm, we come across the step, i, where a_i will exceed c_{i-1}, and for decreasing CZ length we will have $a_i > c_{i-1}$ in all the steps which follow. Thus, for these steps, only one previous value of c (namely c_{i-1}) can be taken as an initial approximation of a_i. To avoid this effect, we will modify the algorithm by fixing $a_i = c_{i-1}$ and computing the corresponding t_i and c_i by solving (6.2) (in the elastic case) or (6.3) (in the viscoelastic case) (setting the crack tip opening displacement equal to the critical crack tip opening) and $K(c_i, t_i) = 0$ (setting the stress intensity factor to zero) respectively. This effectively leads to finer time mesh near the rupture time.

6.3   *Numerical results for the propagating crack*

Choosing PMMA as a reference material, see Appendix A, we used in our numerical examples the value $\delta_c = 0.238$ for the normalised critical crack tip opening.

The graphs in Fig. 12 show coordinates of the crack tip and the CZ tip for both the elastic and viscoelastic cases.

Graphs of the crack tip and the CZ tip coordinate are rather close. Their difference, the CZ length, $l(t) = c(t) - a(t)$, calculated for the time step $h = 4 \cdot 10^{-4}$ is presented in Fig. 13 in the elastic and viscoelastic cases. The maxima of these graphs are reached at the delay times (crack start times), $t_d = 0.00385$ for the elastic case and $t_d = 0.00364$ for the viscoelastic case, for $b = 4$, $\beta = 2$. The CZ length decreases with time, after the crack starts (or shortly after that for some parameters b
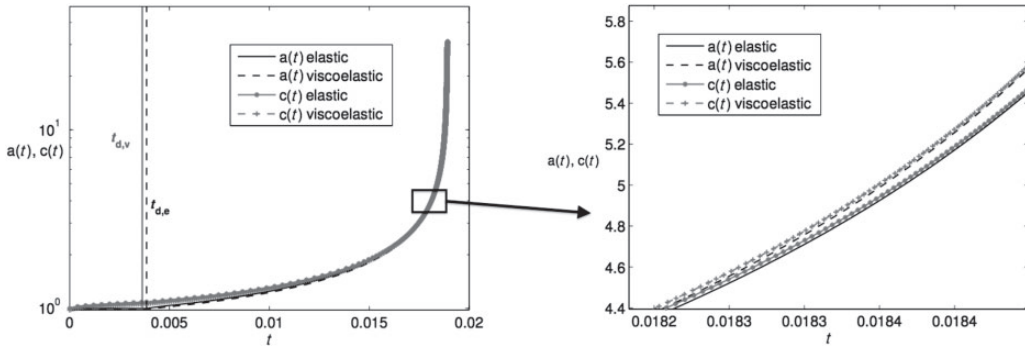

Fig. 12   The crack tip coordinate, $a(t)$, and the CZ tip coordinate, $c(t)$, versus time, t, for $b = 4$, $\beta = 2$
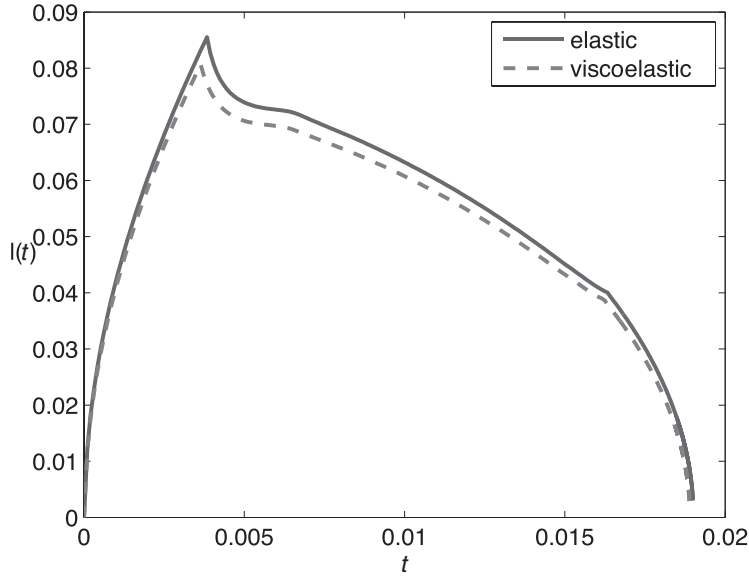
Fig. 13 CZ length, $l(t)$, versus time, t, for $b = 4$, $\beta = 2$

and β), which is surprising at the first glance but not contradictory. Note that the decrease of the CZ length with the increase of crack size has been also observed for other CZ models (**10**, Fig. 4).

The dependence of the CZ length at the crack start, $t = t_d$, as well as of the maximum CZ length (when the maximum is not at $t = t_d$) are given for different parameter sets in Figs 14 and 15. As one can see from Fig. 14, the CZ length can reach maximum not at $t = t_d$ but after the crack starts, for small b.

6.3.1 *Crack start jump analysis.* Let us now analyse what is happening at the onset on crack growth. Considering the graph of the CZ length, $l(t)$, at the vicinity of the delay time, see Fig. 16, we see that for $b = 4$ and $\beta = 1/2$, the CZ length $l(t)$ reaches maximum at the corresponding values of t_d (different for the elastic and viscoelastic cases), while the decrease of the CZ length, as crack growth starts, is more pronounced in the elastic case than in the viscoelastic one. Moreover, by taking other sets of parameters, $b = 4$, $\beta = 1/2$, we observe that the decrease of $l(t)$ at the onset of crack growth is sharper.

To distinguish the effects produced by the model from the numerical artefacts and, particularly to identify the crack evolution instability or otherwise at the crack propagation onset, we will look at the influence of refining the time mesh. Let us consider, how changing the time step size influences the CZ length behaviour obtained numerically. We have 7, 13 and 26 time steps before crack growth for cases $h = 1 \cdot 10^{-3}$, $h = 5 \cdot 10^{-4}$ and $h = 2.5 \cdot 10^{-4}$, respectively. From Fig. 17, we see that the initial decrease in the CZ length is sharper at finer time meshes, for some set of parameters b and β.

To analyse, in a more systematic way, whether the CZ tip coordinate, $c(t)$, crack tip coordinate, $a(t)$, and the CZ length, $l(t) = c(t) - a(t)$, are continuous or discontinuous at $t = t_d$, we calculated their
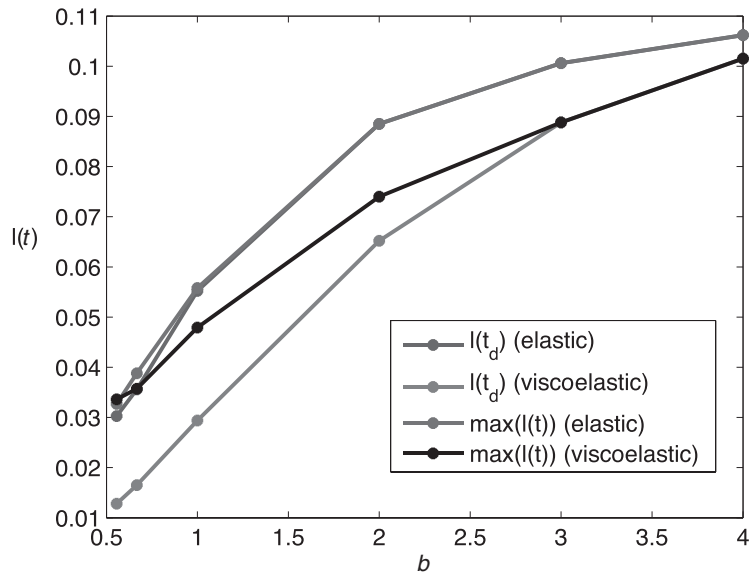
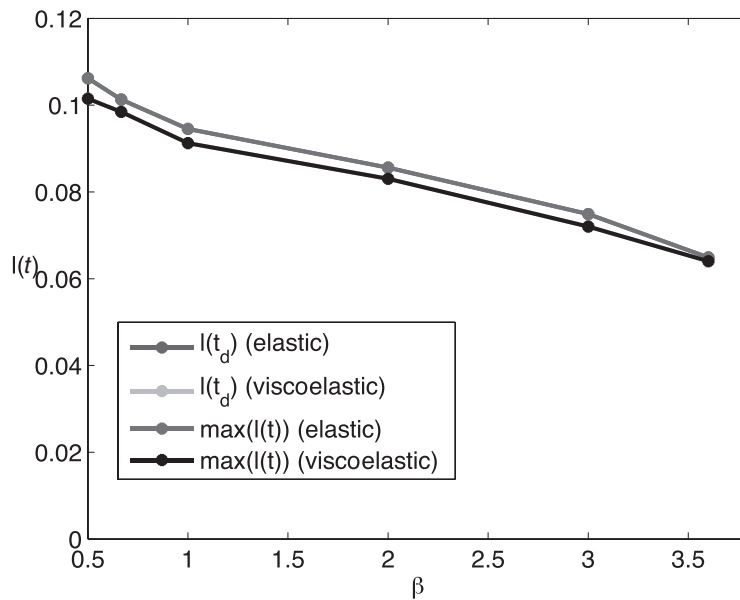**Fig. 14**   CZ length at $t = t_d$ and maximal CZ length, versus b, for $\beta = \frac{1}{2}$

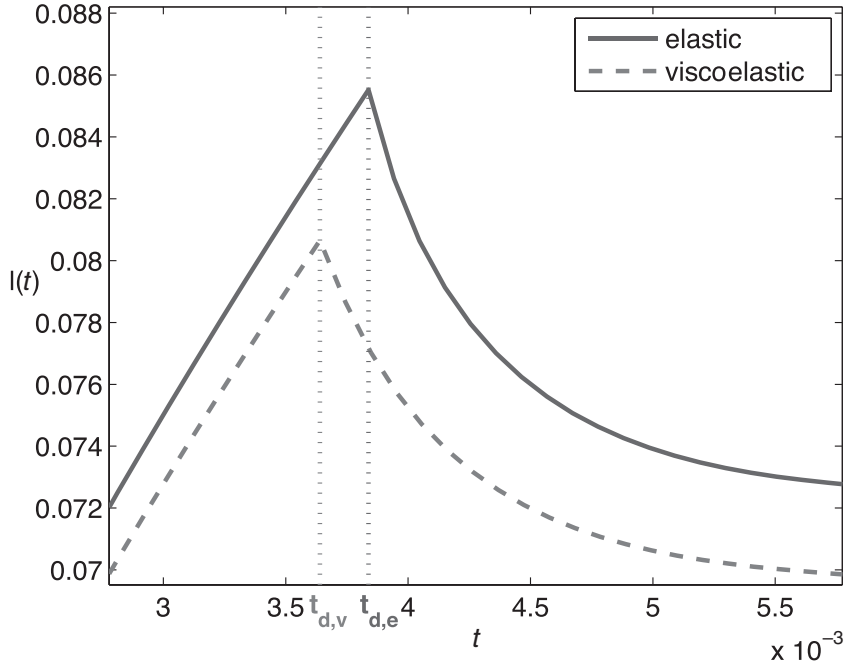**Fig. 15**   CZ length at $t = t_d$, versus β, for $b = 4$

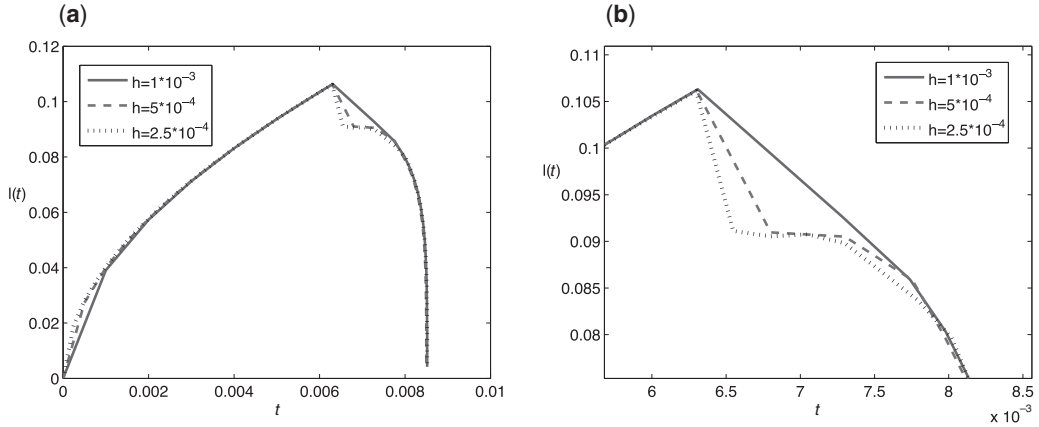**Fig. 16** CZ length, $l(t)$, versus time, t, for $b = 4$, $\beta = 1/2$

Fig. 17 CZ length, $l(t)$, versus time, t, for $b = 4$, $\beta = 1/2$ (elastic)

values at a sequence of points $t_i > t_d$ tending to t_d. The numerical experiment for $b = 4$, $\beta = 1/2$, see Figs 18, 19 and 21, at $h = 2.5 \cdot 10^{-4}$, shows that $a(t_i)$, $c(t_i)$ and $l(t_i)$ tend, respectively to the limiting values $a_{d+} = 1.018 \neq a_0 = 1$, $c_{d+} = 1.112 \neq c(t_d) = 1.106$, and $l_{d+} = 0.0938 \neq l(t_d) = 0.106$.
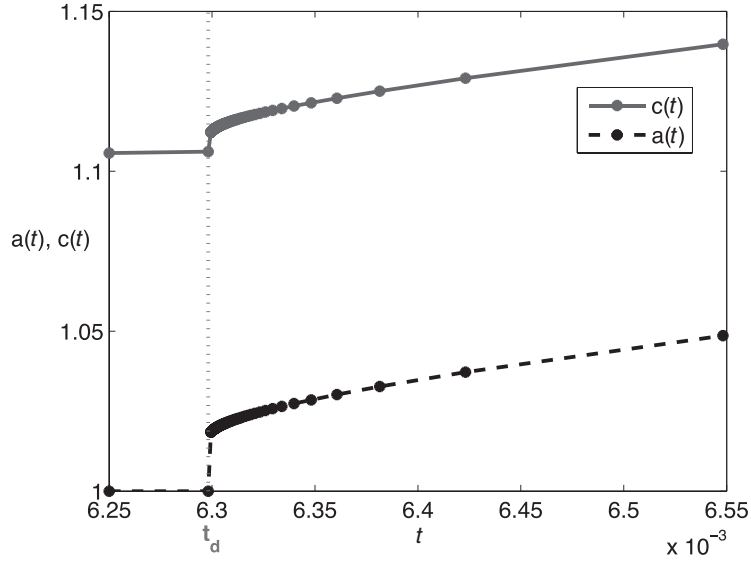
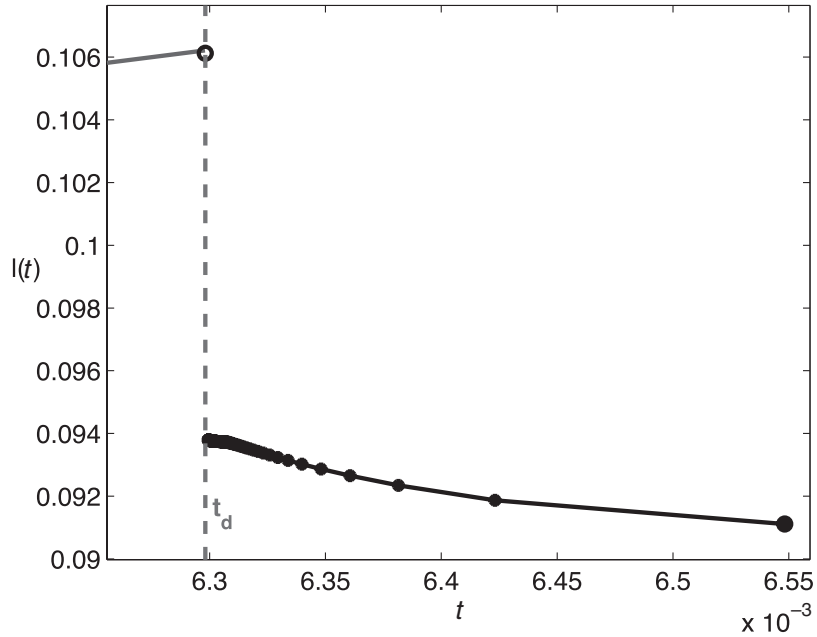**Fig. 18** $a(t)$ and $c(t)$ versus time, t, for $b = 4$, $\beta = 1/2$ (elastic)

Fig. 19 CZ length, l, versus time, t, near t_d for $b = 4$, $\beta = 1/2$ (elastic)
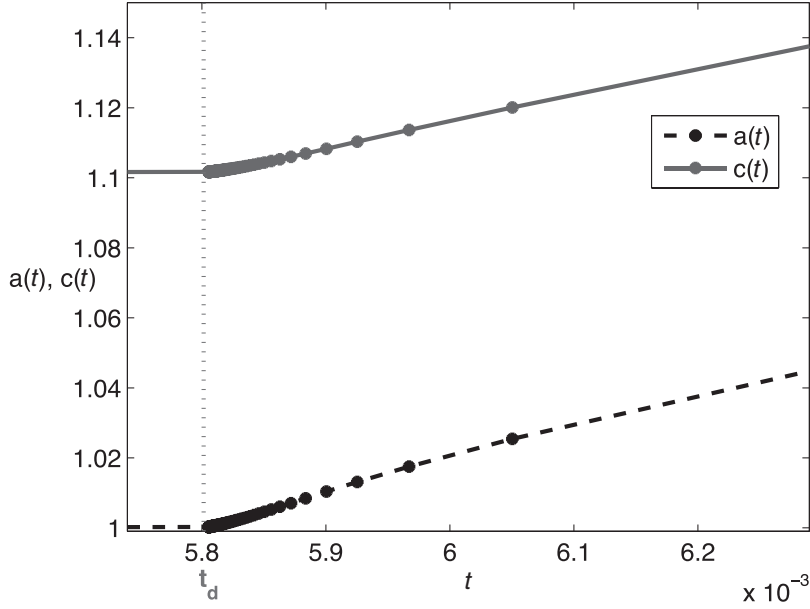
Fig. 20 $a(t)$ and $c(t)$ versus time, t, for $b = 4$, $\beta = 1/2$ (viscoelastic)

The jump of the crack length at $t = t_d$, seen on the figures, indicates that there is an unstable crack growth at the onset of crack propagation followed by the stable crack growth, for the chosen set of parameters, $b = 4$, $\beta = 1/2$, in the elastic case. It causes also a jump decrease in the CZ length followed by a continuous CZ length evolution.

A similar analysis for the viscoelastic case with the same parameters, $b = 4$, $\beta = 1/2$, see Fig. 20, shows that the functions $c(t)$, $a(t)$ and $l(t)$ are continuous at $t = t_d$, unlike in the elastic case.

Figure 21 gives comparison of the evolution of CZ length for elastic and viscoelastic cases for $b = 4$, $\beta = 1/2$.

Figures 22 and 23 show the graphs for the crack tip coordinate, $a(t)$, the CZ tip coordinate, $c(t)$, and the CZ length, $l(t)$, versus time, t, for the value of $b = 18$, which is of the order of the one for PMMA (see Appendix A), and $\beta = b/2 = 9$, in the elastic case. Qualitatively, these graphs are similar to the ones with $b = 4$ discussed earlier. But due to the high value of b, the delay time $t_d = 1.04 \cdot 10^{-10}$ and the rupture time, $t_r = 1.34 \cdot 10^{-10}$ are extremely small in comparison with the rupture time, $t_\infty = 1$, of the material without crack under the same load. Note however that by (2.2) this implies that the rupture time for the plane with crack $a_0 = 1$ equals to the rupture time of the same plane without crack but under the applied load $\hat{q}$ increased in $t_r^{-1/b} \approx 3.5$ times. The corresponding graphs for the viscoelastic case are practically indistinguishable from the elastic ones, Figs 22 and 23, because of the very small times, during which the viscoelastic correction to the purely elastic crack tip opening in (5.8) is insignificant. From the graphs we can also conclude that for the parameters $b = 18$, $\beta = 9$, the unstable crack onset is followed by its stable propagation for both, elastic and viscoelastic cases.
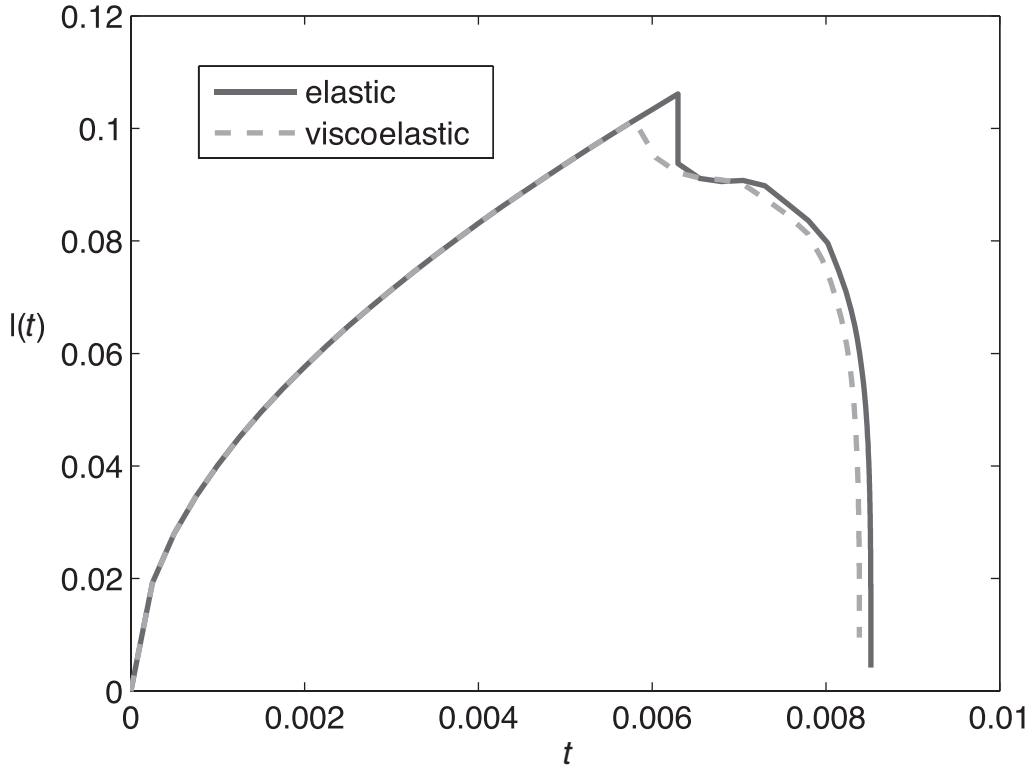
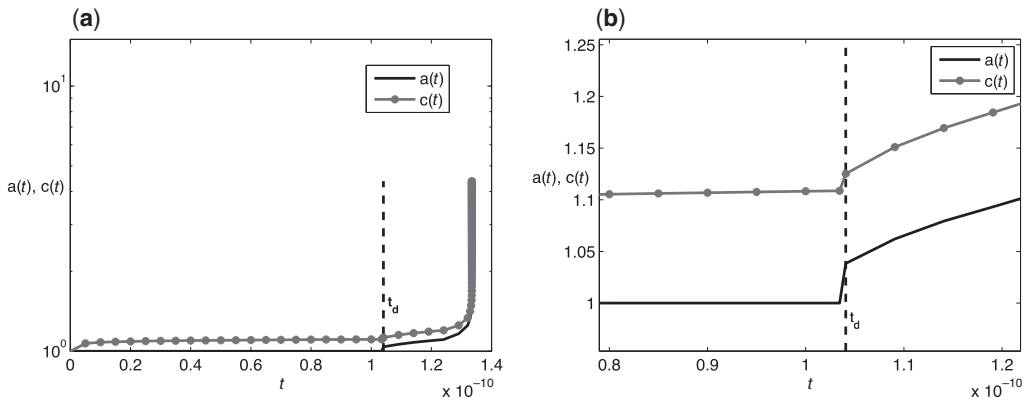**Fig. 21** CZ length, $l(t)$ versus time, t, for $b = 4$, $\beta = 1/2$

Fig. 22 The crack tip coordinate, $a(t)$, and the CZ tip coordinate, $c(t)$, versus time, t, for $b = 18$, $\beta = 9$
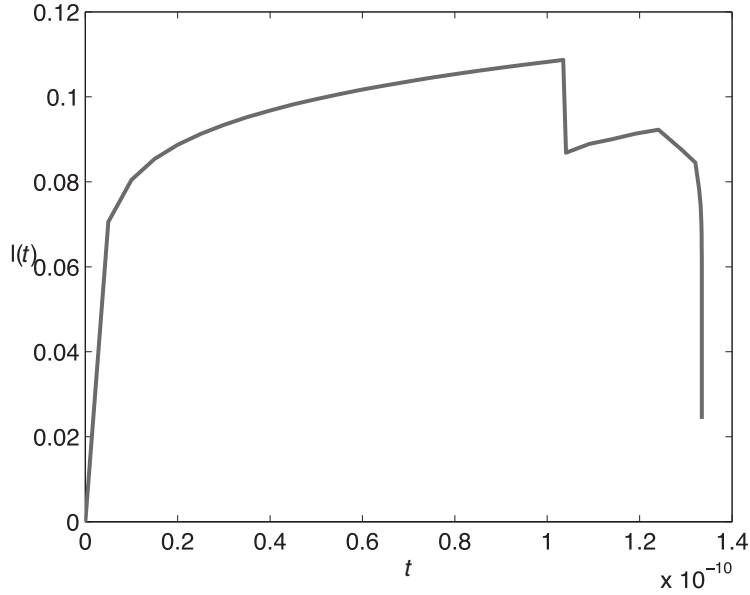
Fig. 23 CZ length, $l(t)$ versus time, t, for $b = 18$, $\beta = 9$

6.3.2 *Delay time and rupture time dependence on b and β.* The rupture time was calculated from the linear extrapolation of the functions $1/c(t)$ and $1/a(t)$, tending to zero at $t = t_r$, which is equivalent to employing the secant method, over the last time step of the algorithm. The values of t_r obtained by these two ways of calculation coincided up to 8 decimal places. Note that the same procedure applied to the function $l(t)$ has also given the same time t_r, which justifies our conclusion that the CZ length, $l(t)$, tends to zero as $t \to t_r$.

The normalised delay time t_d and rupture time of the body (which is the infinite plane in this problem), t_r, depend on the material parameters b and β, and Fig. 24 shows these dependences on b for fixed $\beta = \frac{1}{2}$, whereas Fig. 25 shows the dependences on β for fixed $b = 4$.

The calculations were done for $\beta = \frac{3b}{4}$, $\beta = \frac{b}{2}$, $\beta = \frac{b}{4}$, $\beta = \frac{b}{6}$ and $\beta = \frac{b}{8}$. The data indicate a strong dependence of the normalised rupture time in the infinite plane on the presence of the crack and on the material parameters b and β. This is in contrast to the crack propagation results obtained in the models without the cohesive zone, where the rupture time in the plane with and without crack was the same (**22**, **18**, **19**). The shorter rupture time for the body with existing crack looks more natural, which provides another argument for employing the CZ model.

7. Convergence rates

In the model problems which were numerically solved, we obtained numerical solutions using successively refined meshes. Now we will look at the convergence rate of several computed variables in more details.
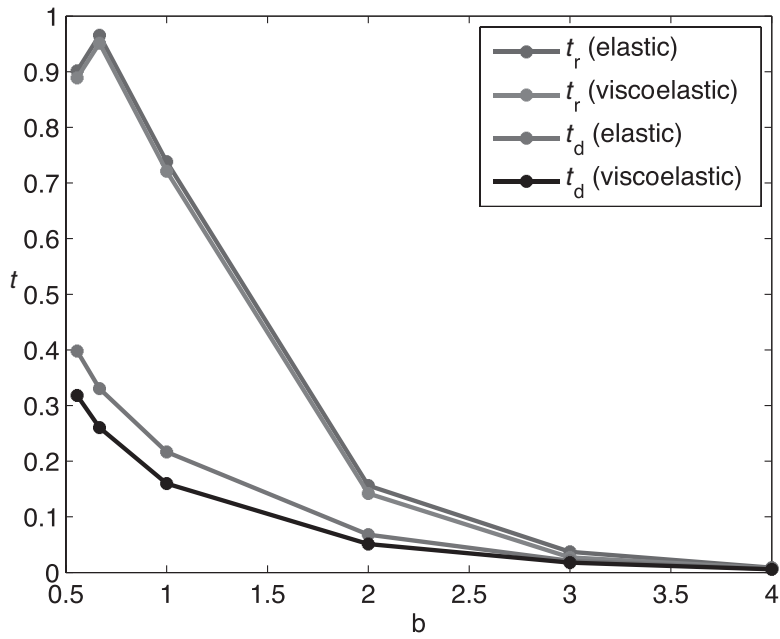
Fig. 24   Delay time, t_d, and rupture time, t_r, versus b, for $\beta = 1/2$
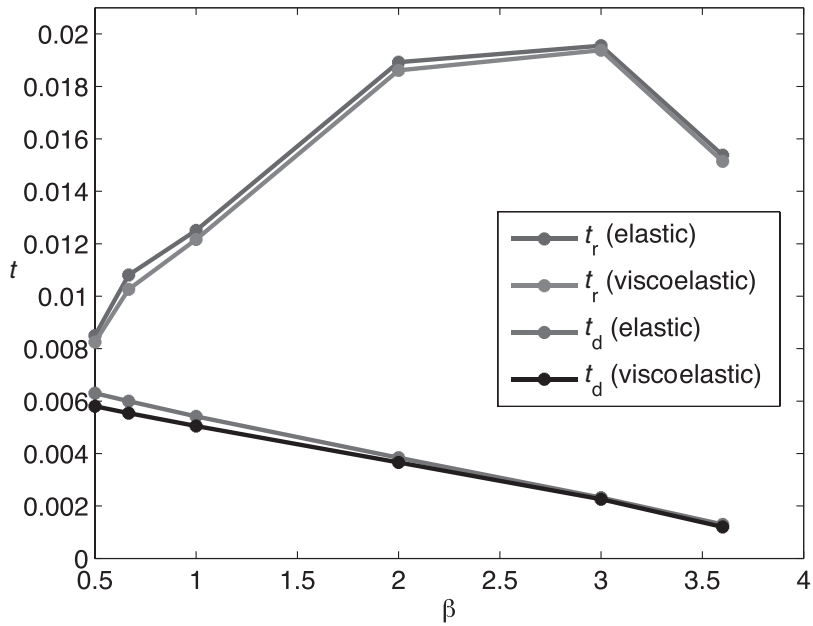

Fig. 25   Delay time, t_d, and rupture time, t_r, versus β, for $b = 4$

Let f denote the exact value of a variable and f_N corresponds to the numerical solution obtained for the step size $h = h_N$, $N = 1, 2, \ldots, N_*$, and

$$\epsilon = \epsilon(f_N) = |f - f_N|$$

denote the corresponding absolute error.

When the exact values are unknown, we will use Aitken's extrapolation technique, also known as the Aitken Δ^2 process, see, for example (**25**, section 2.6), to accelerate the convergence and obtain a good approximation to the exact solution. It gives an approximation f_a of the exact solution f based on three consecutive terms of a convergent sequence,

$$f_a = \frac{f_{N_*} f_{N_*-2} - \left(f_{N_*-1}\right)^2}{f_{N_*} - 2 f_{N_*-1} + f_{N_*-2}}. \tag{7.1}$$

Consequently, the approximate error will be taken as $\epsilon_N \approx |f_a - f_N|$. We assume that there exists a constant C such that $\epsilon_N = C h_N^\alpha$. Then we have

$$\alpha = \frac{\log\left(\epsilon_{N-1}/\epsilon_N\right)}{\log\left(h_{N-1}/h_N\right)}.$$

7.1 Convergence for stationary crack

Taking the time instant $t = 0.6$, we plot in Fig. 26 the error in the CZ length, l, for $b = 4$, $\beta = 2$, versus the time step, h, and present the numerically estimated convergence rate.

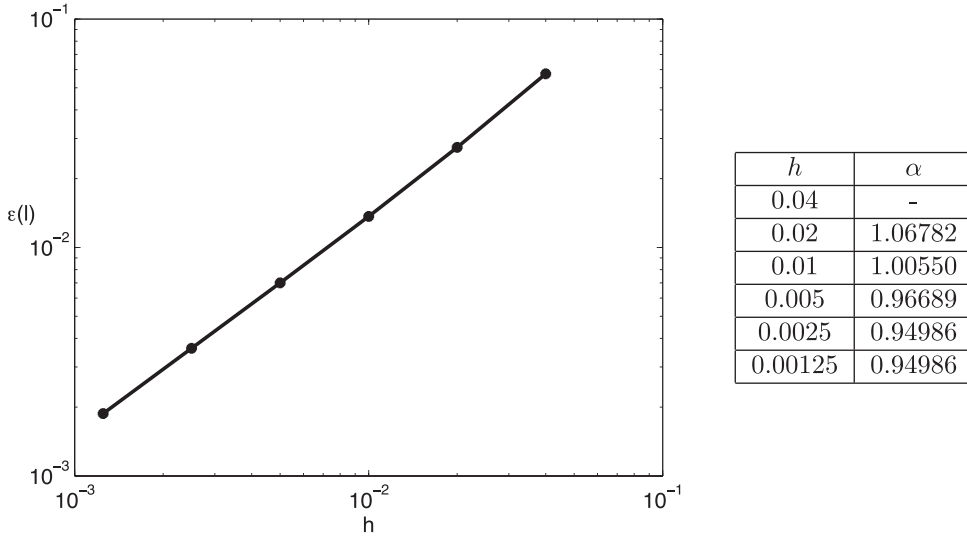| h	α
0.04	–
0.02	1.06782
0.01	1.00550
0.005	0.96689
0.0025	0.94986
0.00125	0.94986

Fig. 26 CZ length error, $\epsilon(l)$, versus time step, h, for $b = 4$, $\beta = b/2$, $t = 0.6$. The table gives the convergence rate for CZ length, l
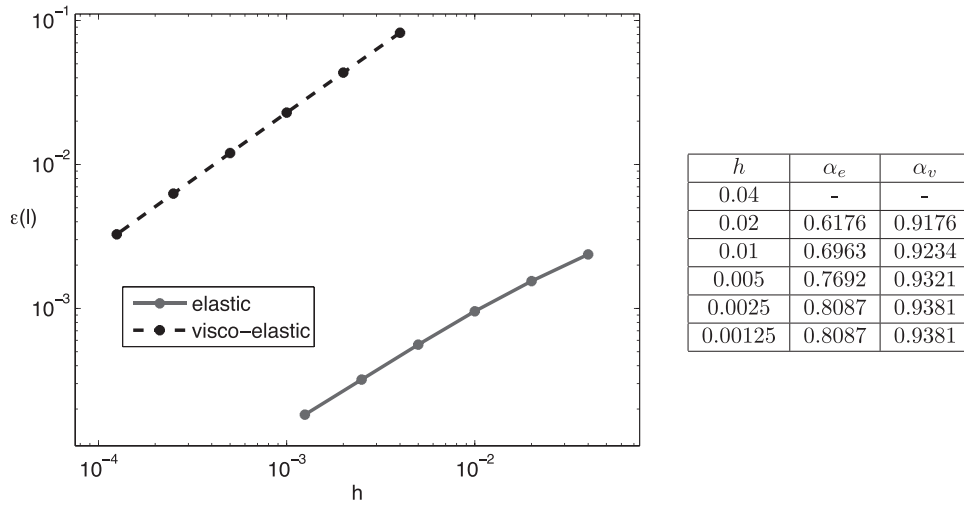
h	α_e	α_v
0.04	-	-
0.02	0.6176	0.9176
0.01	0.6963	0.9234
0.005	0.7692	0.9321
0.0025	0.8087	0.9381
0.00125	0.8087	0.9381

Fig. 27 Crack tip opening error, $\epsilon(\delta)$, versus time step, h, for $b = 4$, $\beta = 2$. The table gives the convergence rates for crack tip opening, δ

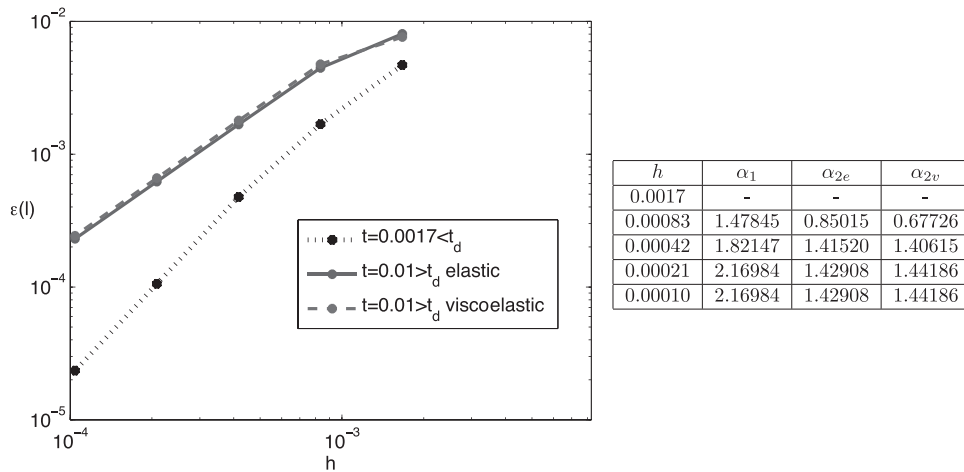| h	α_1	α_{2e}	α_{2v}
0.0017	-	-	-
0.00083	1.47845	0.85015	0.67726
0.00042	1.82147	1.41520	1.40615
0.00021	2.16984	1.42908	1.44186
0.00010	2.16984	1.42908	1.44186

Fig. 28 CZ length error, $\epsilon(l)$, versus time step, h, for $b = 4$, $\beta = 2$. The table gives the convergence rates for the CZ length, l

Figure 27 shows the error, $\epsilon(\delta)$, and the numerical convergence rates, α_e and α_v, of the crack tip opening, δ, for the elastic and the viscoelastic cases, respectively, versus the time step, h.

7.2 *Convergence for propagating crack*

Now, we will compute the convergence rates at time instants before and after the crack-growth start time t_d. Note that the CZ length evolution is the same for the elastic and viscoelastic cases if $t < t_d$. We show the results for $b = 4$, $\beta = 2$, for which, as was mentioned above, $t_d = 0.00385$ for the elastic case and $t_d = 0.00366$ for the viscoelastic case.

Let α_1 denote the numerical convergence rate at $t = 1/600 \approx 0.0017 < t_d$, while α_{2e} and α_{2v} denote the numerical convergence rates, for the elastic and viscoelastic cases respectively, at $t = 0.01 > t_d$. Figure 28 gives graphs of the errors and shows the order of convergence of the CZ length.

A more detailed *a posteriori* analysis of convergence in considered numerical examples is available (**23**).

8. Concluding remarks

A novel nonlinear history-dependent CZ model of crack propagation in linearly elastic and viscoelastic materials, which is a history-dependent modification of the LPD model, was introduced in the article. The normal stress on the CZ satisfies the history-dependent yield condition, given in terms of the normalised history-dependent equivalent stress (2.1), which is a nonlinear Abel-type integral operator, implemented before in (**15**) as a (global) material strength condition. The viscoelasticity is described by a linear Volterra integral operator in time. The crack starts propagating, breaking the CZ, when the crack tip opening reaches a prescribed critical value. A numerical algorithm for computing the evolution of the crack and cohesive zone in time is discussed along with some numerical results.

As was shown in the article, the CZ model is applicable only if material parameters, b and β, of the history-dependent yield condition, based on the power-type durability diagram, are such that $b > 0$, $0 < \beta < b$. This particularly implies that the CZ model is not applicable for the Robinson-type yield condition, based on the power-type durability diagram.

The numerical results have shown that for both, elastic and viscoelastic materials, there exists a fracture delay time t_d, after a remote constant load is applied, during which the CZ grows while the crack does not.

For the growing crack stage, $t > t_d$, the crack growth rate increases, while the CZ length decreases, with time. It appeared that, for some material parameters, there is an unstable crack growth at the onset of crack propagation, followed by stable crack growth. It also causes a jump decrease in the CZ length followed by a continuous CZ length evolution. However, for other material parameters, no crack instability was detected, implying the stable crack propagation. These numerically observed effects provide a motivation for a theoretical analysis of crack stability/instability in history-dependent materials, after the crack growth start.

The time, when the CZ length decreases to zero coincides with the time when the crack length becomes infinite and can be associated with the complete rupture of the body, the rupture time. The rupture time for the viscoelastic case is slightly smaller than that for the purely elastic case.

Implementing different mesh sizes we observed that the solution, normally, converges with the mesh refinement. An exception is the very slow (if at all) convergence of the CZ tip stress, for some material parameters, which may be a manifestation of a CZ tip stress singularity. Although the square root singularity has been eliminated in the model by the requirement that the corresponding stress intensity factor at the CZ tip is zero, a singularity of a different order can be still present there, however this needs a careful analysis, which is beyond the scope of this article.

The results presented in the article particularly show that the normalised history-dependent equivalent stress (2.1) is well suitable not only for better approximation of the experimental creep strength data, see (15), but can also be successfully used for the numerical solution of some non-stationary problems for bodies under inhomogeneous variable stresses.

To predict the strength of the material and the point where fracture will occur, a local or non-local approach can be used. The local approach employs the stress (or stress history) at a point, while the non-local approach uses the stress (history) not only at the point but also in its vicinity. As shown in (26), the cohesive zone model approach can be also interpreted as a particular non-local approach (27, 28). In this sense, the CZ model in history-dependent materials presented in this paper is related to another non-local approach based on the Neuber-Novozhilov type stress averaging ahead of the crack under creep or fatigue loading (22, 18). As for the materials without time and history dependence, the CZ model looks more mechanically justified, but its numerical implementation is more involved analytically and numerically than for other non-local models.

The obtained numerical results for the crack length dependence on time are qualitatively similar to the experimental results and some other model predictions available in (4, 29). To make quantitative comparison, one needs the data on the bulk material durability in addition to the ones usually provided in the papers, and the authors hope to do such comparison, when the data will be available to them.

The model problem presented in this article could be extended in various ways. For example, the history-dependent CZ model could be implemented in three-dimensional problems with a penny-shaped crack containing a cohesive region around the circumference, revising the setting in (4). For more general problems, when there is no analytic solution for the bulk of material, the history-dependent CZM can be used in conjunction with general numerical methods like Boundary Element Method, Finite Element Method, Mesh Free Methods, etc. (17, 30).

References

1. D. S. Dugdale, Yielding of steel sheets containing slits, *J. Mech. Phys. Solids* **8** (1960) 100–104.

2. M. Ya. Leonov and V. V. Panasyuk, Development of the smallest cracks in the solid (Russian), *Prikladnaya Mekhanika* **5** (1959) 391–401.

3. D. Gross and T. Seelig, *Fracture Mechanics* (Springer, Heidelberg 2011).

4. M. P. Wnuk and W. G. Knauss, Delayed fracture in viscoelastic-plastic solids, *Int. J. Solids Struct.* **6** (1970) 995–1009.

5. R. A. Schapery, Correspondence principles and a generalized J integral for large deformation and fracture analysis of viscoelastic media, *Int. J. Fract.* **25** (1984) 195–223.

6. G. I. Barenblatt, The formation of equilibrium cracks during brittle fracture. General ideas and hypotheses. Axially-symmetric cracks, *J. Appl. Math. Mech.* **23** (1959) 622–636.

7. G. I. Barenblatt, Equilibrium cracks formed during brittle fracture. Rectilinear cracks in plane plates, *J. Appl. Math. Mech.* **23** (1959) 1009–1029.

8. G. I. Barenblatt, The mathematical theory of equilibrium cracks in brittle fracture, *Adv. Appl. Mech.* **7** (1962) 55–129.

9. L. N. McCartney, Crack-growth predictions for viscoelastic materials exhibiting non-uniform craze deformation, *Int. J. Fract.* **37** (1988) 279–301.

10. W. G. Knauss, Time dependent fracture and cohesive zones, *J. Engng. Materials and Tech.* **115** (1993) 262–267.

11. W. G. Knauss and G. U. Losi, Crack propagation in a nonlinearly viscoelastic solid with relevance to adhesive bond failure, *J. Appl. Mech.* **60** (1993) 793–801.

12. C. Yoon and D. H. Allen, Damage dependent constitutive behavior and energy release rate for a cohesive zone in a thermoviscoelastic solid, *Int. J. Fract.* **96** (1999) 55–74.

13. Z. P. Bažant and Y.-N. Li, Cohesive crack with rate-dependent opening and viscoelasticity: I. Mathematical model and scaling, *Int. J. Fract.* **86** (1997) 247–265.

14. Y. N. Li and Z. P. Bažant, Cohesive crack model with rate-dependent opening and viscoelasticity: II. Numerical algorithm, behavior and size effect, *Int. J. Fract.* **86** (1997) 267–288.

15. S. E. Mikhailov and I. V. Namestnikova, History-sensitive accumulation rules for life-time prediction under variable loading, *Arch. Appl. Mech.* **81** (2011) 1679–1696.

16. L. Hakim and S. E. Mikhailov, Integral equations in cohesive zones modelling of fracture in history dependent materials, *Proc. World Congress on Engineering 2013* (Newswood Limited, International Association of Engineers, 2013), 226–231.

17. D. H. Allen and C. R. Searcy, A micromechanical model for a viscoelastic cohesive zone, *Int. J. Fract.* **107** (2001) 159–176.

18. S. E. Mikhailov and I. V. Namestnikova, Local and non-local approaches to creep crack initiation and propagation, *Proc. 9th International Conference on the Mechanical Behaviour of Materials*, Geneva, Switzerland, 2003.

19. L. Hakim and S. E. Mikhailov, Nonlinear Abel type integral equation in modelling creep crack propagation, *Integral Methods in Science and Engineering* (ed. C. Constanda and P. Harris, Springer (Birkhäuser), Boston, 2011) 191–201.

20. N. I. Muskhelishvili, *Some Basic Problems of the Mathematical Theory of Elasticity* (Noordhoff, Groningen 1954).

21. R. Gorenflo and S. Vessella, *Abel Integral Equations Analysis and Applications* (Springer, Berlin 1991).

22. S. Mikhailov and I. Namestnikova, Local and non-local approaches to fatigue crack initiation and propagation, *Proc. IUTAM Symposium on Singularities, Asymptotics and Homogenisation in Problems of Mechanics* (ed. A. Movchan, Kluwer, New York, 2003), 285–294.

23. L. Hakim, Numerical Implementation of a cohesive zone model for time and history dependent materials. PhD Thesis (2014, Brunel University, London).

24. Yu. N. Rabotnov, *Elements of Hereditary Solid Mechanics* (Mir Publishers, Moscow 1980).

25. K. E. Atkinson, *An Introduction to Numerical Analysis* (Willey, New York 1989).

26. S. E. Mikhailov, Non-local strength conditions based on generalized δ_c cohesive models, *Zeit Angew. Math. Mech.* **80** (2000) S483–S486.

27. S. E. Mikhailov, A functional approach to non-local strength conditions and fracture criteria: I. Body and point fracture, *Eng. Fract. Mech.* **52** (1995) 731–743.

28. S. E. Mikhailov, A functional approach to non-local strength conditions and fracture criteria: II. Discrete fracture, *Eng. Fract. Mech.* **52** (1995) 745–754.

29. W. G. Knauss, Delayed failure – The Griffith problem for linearly viscoelastic materials, *Int. J. Fract. Mech.* **6** (1970) 7–20.

30. T. Rabczuk, P. M. A. Areias and T. Belytschko, A simplified meshfree method for shear bands with cohesive surfaces, *Int. J. Num. Meth. Engng.* **69** (2007) 993–1021.

31. J. E. Mark, *Polymer Data Handbook* (Oxford University Press, New York 1999).

32. H. Kobayashi, H. Takahashi and Y. Hiki, Viscosity measurement of organic glasses below and above glass transition temperature, *J. Non-Crystalline Solids* **290** (2001) 32–40.

33. B. Cotterell, *Fracture and Life* (World Scientific, Singapore 2010).

34. G. B. McKenna and J. M. Crissman, A reduced variable approach to relating creep and creep rupture in PMMA, *MRS Proceedings* **79** (1986) 333–343.

APPENDIX A

Material parameters used in the numerical examples

In this paper we used material parameters close to those for PMMA. For the rheological parameters we took (see (**31**, pp. 655–657) and (**32**, **33**)): Poisson's ratio $\nu = 0.35$; Young's modulus $E_0 = 3100$MPa (hence $\mu_0 = 1148$MPa); viscosity $\eta = 2 \cdot 10^7$ MPas. We also chose $\hat{\theta} = 3.23 \cdot 10^4$ s.

Fitting the creep rupture data under tensile stress for PMMA from (**34**) gives the values $b = 18.5$ and $\hat{\sigma}_0 = 58.1$MPa hr$^{1/b}$ in the durability curve (6.1). Taking the applied load $\hat{q} = 51.6$MPa, we arrive at the values $\hat{t}_\infty = 8.96$hr, $m = 5$ and $\theta = 1$.

We took the critical crack opening displacement $\hat{\delta}_c = 0.0016$mm, see (**33**, section 10.3.2) and references therein. Under the plane stress condition $\varkappa = (3 - \nu)/(1 + \nu) = 1.96$ and by (6.1) we obtain $\delta_c = 0.238$ for $\hat{q} = 51.6$MPa and for the initial crack length $\hat{a}_0 = 0.1$mm.

APPENDIX B

Continuity of $\sigma(x, t)$ in t

Let us analyse the behaviour of the numerical solution of (2.7) for $\sigma(x, t)$ as $t \to t_c(x) + 0$ and prove that if we take the piecewise approximation of the function $\sigma^\beta(x, t)$ in $t \le t_c(x)$ over the time instants $t_j, j = 0, 1, 2, \ldots, k$, we obtain continuity of $\sigma^\beta(x, t)$ at $t = t_c(x)$ also from the right, that is, when $t \to t_c(x) + 0$.

Indeed, from the first equality in (4.3), where $t_k = t_c(x)$, we have,

$$
\lim_{t \to t_c(x)+0} \sigma^\beta(x, t) = \lim_{t \to t_c(x)+0} \frac{-1}{\pi} \sin(\pi\gamma) \Bigg[\sum_{j=1}^{k} \sigma^\beta(x, t_{j-1}) \left(V(t_{j-1}, t, t_c(x)) - V(t_j, t, t_c(x)) \right)
$$

$$
+ \frac{1}{\gamma} \left(\frac{\sigma^\beta(x, t_j) - \sigma^\beta(x, t_{j-1})}{t_j - t_{j-1}} \right) \left(W(t_{j-1}, t, t_c(x)) - W(t_j, t, t_c(x)) - \gamma(t_j - t_{j-1})V(t_j, t, t_c(x)) \right) \Bigg]. \quad \text{(B.1)}
$$

In the above formula, only $V(y, t, t_c(x))$ and $W(y, t, t_c(x))$ depend on t. Moreover, since $\beta > 0$, from (4.4) and (4.7) we have for any t,
$$
V(t_c, t, t_c) = \pi \csc(\pi\gamma), \quad W(t_c, t, t_c) = 0.
$$

For the case when $y \ne t_c$, we have

$$
\lim_{t \to t_c+0} V(y, t, t_c) = \lim_{t \to t_c+0} \left\{ \pi \csc(\pi\gamma) - \frac{1}{\gamma} \left(\frac{t_c - y}{t - y} \right)^\gamma \, {}_2F_1\left(\gamma, \gamma; 1 + \gamma; \frac{t_c - y}{t - y} \right) \right\}
$$

$$
= \pi \csc(\pi\gamma) - \gamma^{-1}\Gamma(1 + \gamma)\Gamma(1 - \gamma) = 0,
$$

$$
\lim_{t \to t_c+0} W(y, t, t_c)
$$

$$
= \lim_{t \to t_c+0} \left\{ \gamma\pi \csc(\pi\gamma)(t - y) - \frac{1}{1 + \gamma}(t_c - y)^{1+\gamma}(t - y)^{-\gamma} \, {}_2F_1\left(1 + \gamma, \gamma; 2 + \gamma; \frac{t_c - y}{t - y} \right) \right\}
$$

$$
= \gamma\pi \csc(\pi\gamma)(t_c - y) - (1 + \gamma)^{-1}(t_c - y)\Gamma(2 + \gamma)\Gamma(1 - \gamma) = 0,
$$

where we have used

$$
{}_2F_1(a, b; c; 1) = \frac{\Gamma(c)\Gamma(c - a - b)}{\Gamma(c - a)\Gamma(c - b)}
$$

and other properties of the Gamma function such as $\Gamma(z + 1) = z\Gamma(z)$ and $\Gamma(1 - z)\Gamma(z) = \pi \csc(\pi z)$.

Consequently, in (B.1), the summation over j yields

$$\lim_{t \to t_c(x)+0} \sigma^\beta(x, t) = -\frac{1}{\pi} \sin(\pi\gamma)\left[-\pi \csc(\pi\gamma)\sigma^\beta(x, t_{k-1}) \right.$$

$$\left. +\frac{1}{\gamma} \cdot \frac{\sigma^\beta(x, t_c(x)) - \sigma^\beta(x, t_{k-1})}{t_c(x) - t_{k-1}} \left(\gamma(t_c(x) - t_{k-1})\pi \csc(\pi\gamma)\right) \right] = \sigma^\beta(x, t_c(x)).$$

Therefore, $\lim_{t \to t_c(x)+0} \sigma^\beta(x, t) = \sigma^\beta(x, t_c(x))$ for $0 < \gamma < 1$.